12-2014

# NUMERICAL SIMULATION OF THE HEAT LEAKAGE AT THE GASKET REGION OF DOMESTIC REFRIGERATORS

Feng Gao
*Clemson University*, fgao2@g.clemson.edu

# NUMERICAL SIMULATION OF THE HEAT LEAKAGE AT THE GASKET REGION OF DOMESTIC REFRIGERATORS

---

A Thesis
Presented to
the Graduate School of
Clemson University

---

In Partial Fulfillment
of the Requirement for the Degree
Master of Science
Mechanical Engineering

---

by
Feng Gao
December 2014

---

Advisor: Dr. Richard S. Miller, Committee Chair
Dr. John R. Wagner
Dr. Xiangchun (Schwann) Xuan

## ABSTRACT

Computational Fluid Dynamics (CFD) simulations are performed to investigate the heat loss at the gasket of a standard over/under domestic refrigerator. The study numerically simulates a unique experimental test cell with only the gasket region exposed to the ambient environment and other parts protected by insulation (see picture below). The test cell is cubic with an interior cavity having dimensions 2’ x 2’ x 2’ within which a heating element is placed to create a specified temperature difference. A matching set of door and side panels exposes a 2’ width of the gasket region to heat transfer with the surroundings. The primary objectives are to obtain the effective heat leakage in energy leakage per unit time, per unit length along the gasket, and per degree of temperature difference across the gasket (eg.W/m·K) and to be able to distinguish differences in heat leakages between different gaskets. To do so requires measuring the heat flux rate exiting the gasket region continuously along the surface normal to the gasket. However, only six experimental measurement locations were possible. Therefore, CFD was performed to provide “shape profiles” which can be used to best fit the experimental data via a Least Mean Square Error approach. These then provide the continuous heat flux profiles which are then numerically integrated to obtain the desired heat leakage.

The commercial ANSYS/Fluent CFD package is employed for the simulations which include both the inner air as well as conduction through all solid materials. A standard

Boussinesq approximation is used in modeling the natural convection and air flow in the chamber of the test cell. The CFD shape profiles are shown to be in good agreement with the experimental data and to collapse well when non-dimensionalized.

Additional simulations are also performed to test the relative impact on heat leakage from additional effects that are either not possible to include or control in the experiments. Simulations that include an electric fan in the chamber show that the heat transfer increases 22 % because of the addition of forced convection. The estimated heat loss at the gasket region increases 11 % when radiation is considered in the simulation with the Discrete Ordinate Method (DOM). The influence of the hot pipe in the freezer compartment is estimated by simulations under actual refrigerator conditions and the numerical results show that the heat loss at the gasket increases 18 % when the hot pipe is in operation.

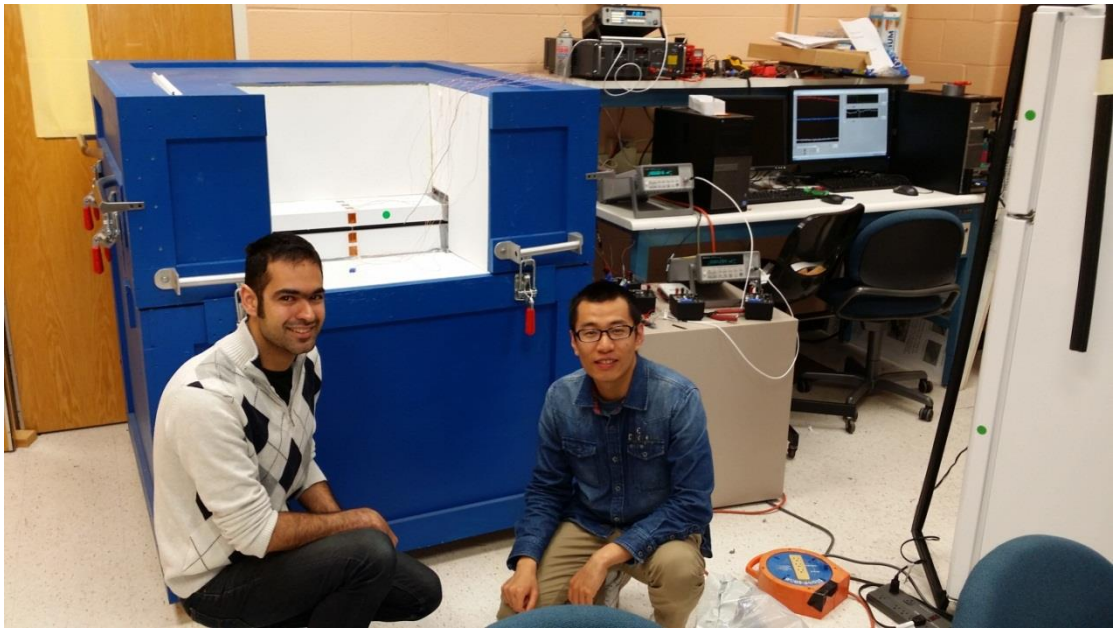

## ACKNOWLEDGMENTS

I would like to dedicate my sincere thanks to my advisor Dr. Miller, who has patiently instructed me throughout my graduate study. With his kindness and professional knowledge, I learned not only about knowledge in a specific engineering field, but more importantly the methods of critical thinking and prudent attitude that are essential for scientific research.

I would also like to thank Dr. John Wagner and Dr. Xiangchun Xuan, who have patiently reviewed my paper and given me valuable and professional advice. I am very thankful to them for serving on my committee.

Mr. Shervin Shoai Naini has provided me great help during the process of my research. It has been a privilege to work with him and I treasure the friendship we have developed through working together.

Most importantly, I would like to dedicate this thesis to the greatest treasure in my life --- my parents, who unconditionally love and support me all the time, especially during my graduate study in the U.S. I could never be thankful enough for their patience, understanding and encouragement. I am genuinely thankful to them for their love from the bottom of my heart.

## TABLE OF CONTENTS

Page

**TITLE PAGE** ..... **i**
**ABSTRACT** ..... **ii**
**ACKNOWLEDGEMENTS** ..... **iv**
**LIST OF FIGURES** ..... **vii**
**LIST OF TABLES** ..... **ix**
**CHAPTER 1: INTRODUCTION** ..... **1**
1.1 Previous Research on the Heat Loss at the Door Gasket of the Refrigerator ..... 4
1.2 CFD Simulation of the Airflow within the Chamber of a Refrigerator ..... 4
1.2.1 Static Type of Refrigerator (without Fan) ..... 6
1.2.2 Ventilated Type of Refrigerator (with Fan) ..... 7
1.3 Reverse Heat Load Method (RHLM) ..... 8
1.4 The Objective of the Present Study ..... 8
**CHAPTER 2: NATURAL CONVECTION SIMULATION** ..... **10**
2.1 The Geometry of the Simulation Domain ..... 10
2.2 Material Properties used in the Present Study ..... 13
2.3 Natural convection (Boussinesq Model) ..... 14
2.4 Boundary Conditions for Natural Convection Simulation ..... 15
2.5 Mesh Quality ..... 17
2.6 Convergence Criteria ..... 18
**CHAPTER 3: FORCED CONVECTION SIMULATION** ..... **21**
3.1 Modification of the Geometry ..... 21
3.2 The Choice and Application of Turbulence Models ..... 22
3.3 Boundary Conditions for Forced Convection ..... 25
3.4 Y+ Values ..... 25
**CHAPTER 4: RADIATION HEAT TRANSFER SIMULATION** ..... **28**
**CHAPTER 5: THE MODELING OF THE HOT PIPE** ..... **30**
**CHAPTER 6: DIFFERENT TYPES OF GASKETS USED** ..... **31**
7.1 Simulation Results of Natural Convection with Heat Load of 9.2 W and 15.0W . 32
7.2 Simulation Results of Forced Convection with 9.2 W Heat Load ..... 36
7.3 Simulation Results including Radiation Heat Transfer with Discrete Ordinate Method (DOM) ..... 41
7.4 Simulation Results of the Heat Loss for Gasket 2 and 3 under the Condition of Natural Convection ..... 43
7.5 Simulation Results of a Hot Pipe in the Test Cell ..... 49

## TABLE OF CONTENTS (CONTINUED)

Page

7.6 The “Best Fit” Shape Profile Generated from the Simulations ..... 54
**CHAPTER 8: CONCLUSIONS ..... 58**
**APPENDIX ..... 59**
**BIBLIOGRAPHY ..... 62**

## LIST OF FIGURES

Page

Figure 1: The (a) test cell interior with the heater inside the chamber, and (b) exposed gasket region with the test cell sealed. ..... 11
Figure 2: The (a) 2D simulation domain of the test cell. The orange rectangular indicates the heater, and (b) a zoom in of the 2D CFD domain of interest showing different surface and interior paths for which the heat flux is to be simulated. ..... 12
Figure 3: The gasket region of the test cell and the implementation of boundary conditions for natural convection. ..... 16
Figure 4: Example mesh of the gasket region generated in ANSYS MESH 14.0. ..... 18
Figure 5: The exemplary of the monitor of the convergence of the CFD simulation. ..... 19
Figure 6: The geometry modification with the electric fan installed. The mean velocity of the air coming out of the electric fan is measured to be 1.1 m/s by using a hot wire anemometer. ..... 21
Figure 7: The surfaces of the wall and the door of the freezer. ..... 27
Figure 8: The measurement of the emissivity of the test cell with a thermal imaging camera. ..... 28
Figure 9: The zoomed in hot pipe (green circle) at the gasket region of the refrigerator. 30
Figure 10: Three types of door gaskets used in simulations. ..... 31
Figure 11: The temperature contour of natural convection with 9.2 W heater energy supply. ..... 33
Figure 12: The velocity contour of natural convection 9.2 W heater energy supply. ..... 34
Figure 13: The temperature contour of natural convection with 15 W heater energy supply. ..... 35
Figure 14: The velocity contour of natural convection with 15 W heater energy supply. 36
Figure 15: The temperature contour forced convection with 9.2 W heater energy supply. ..... 37
Figure 16: The velocity contour of forced convection with 9.2 W heater energy supply. 38
Figure 17: The plot of y+ values of the wall with 9.2 W heater power. ..... 39
Figure 18: The plot of y+ values of the door with 9.2 W heater energy power. ..... 40
Figure 19: The temperature contour of natural convection with 9.2 W heater energy supply (including the DOM radiation heater transfer model). ..... 42
Figure 20: The velocity contour of natural convection with 9.2 W heater energy supply (including the DOM radiation heat transfer model). ..... 43
Figure 21: The temperature contour of natural convection with 9.2 W heater energy supply (Gasket 2). ..... 44

## LIST OF FIGURES (CONTINUED)

Page

Figure 22: The velocity contour of natural convection with 9.2 W heater energy supply (Gasket 1). ..... 45
Figure 23: The zoomed in temperature contour of Gasket 2 with natural convection, 9.2 W heater energy supply. ..... 46
Figure 24: The temperature contour of natural convection with 9.2 W heater energy supply (Gasket 3). ..... 47
Figure 25: The velocity contour of natural convection with 9.2 W heater energy supply (Gasket 3). ..... 48
Figure 26: The zoomed in temperature contour of Gasket 3 with natural convection, 9.2 W heater energy supply. ..... 49
Figure 27: The temperature contour of the test cell with the hot pipe off. ..... 51
Figure 28: The zoomed in temperature contour at the gasket region with the hot pipe off. ..... 52
Figure 29: The temperature contour of the test cell with the hot pipe on. ..... 53
Figure 30: The zoomed in temperature contour at the gasket region with the hot pipe on. ..... 54
Figure 31: The coordinate used along the gasket region. The solid orange line represents the outer surface of the gasket region, whose origin is fixed at point A. The coordinate along the surface of the gasket region is “s”. The location of the six heat flux sensors are placed along the s coordinate at locations 0.03 m, 0.09 m, 0.192 m, 0.258 m and 0.303 m. ..... 55
Figure 32: The plot of the continuous heat flux profile obtained from numerical simulations and experimental data measured by six heat flux sensors along the gasket region surface. (The experimental data is the courtesy from Mr. Shervin Shoai Naini.) ..... 56
Figure 33: The "best fit" profile obtained by LMSE method. s* is obtained by dividing the position of the continuous points (s) by the length of the gasket region (l). ..... 57

## LIST OF TABLES

Page

Table 1: The thermal properties of the materials used in the present numerical simulations. ..... 13
Table 2: Simulated heat leakage for two different heat loads showing the linearity of the heat leakage with temperature difference. ..... 32
Table 3: Effect of the electric fan on the heat leakage through the gasket region. ..... 36
Table 4: Comparison of the heat loss at the gasket between under the conditions of natural convection and radiation heat transfer. ..... 41
Table 5: The comparison of the heat loss at the gaskets between different types of gaskets used in the simulations. ..... 43
Table 6: The comparison of the heat leakage at the gasket between the simulations with the hot pipe on and off. ..... 50

# CHAPTER 1: INTRODUCTION

Refrigerators are one of the most widely used electronic appliances and are held to strict energy efficiency ratings. Hence, investigating the heat loss of the refrigerator system is of great practical meaning. Some researchers [1, 2, 3] have investigated the influence of multiple variables on the energy consumption of refrigerators. However, not much attention has been focused on the heat loss at the door gasket of the refrigerator; although it is acknowledged that it contributes to a significant percentage of the energy consumption of the refrigerator and freezer.

The open literature related to the heat transfer at the door gasket is quite limited and it is not universally agreed upon how much percentage of the heat loss is due to the door gasket and the surrounding regions. In addition, the study approach used by different researchers and the technical specification of refrigerators used in experiments are quite different.

According to a report presented by the EPA [4], the heat loss at the door gasket accounts for around 10 % to as much as 30%. The research of Boughton [5] indicates that the heat loss “at edges” of the refrigerator accounts for about 30% of the total energy consumption. By using the Finite Element Analysis (FEA) method, Shirley and Keith [6] indicate that the gasket region accounts for about 25% of the thermal load into the refrigerator chamber. The figure can increase to 35% if the doors and walls of the refrigerator are of super insulation material. Hasanuzzaman [7] shows that the heat transfer

at the door gasket accounts for about 29% of the total energy consumption by investigating the influence of the operation variables of refrigerator experimentally. Mir-Akbar and Hilligweg [8] estimate that the heat transfer though the door seal is about 13% of the total thermal load by the reverse heat loss method (RHLM) by experimenting on a 370 L capacity domestic refrigerator. They confirm the conclusion by a separate experimental device. Similarly, the research of Wei and Jyi [9] shows that the heat loss at the door gasket of the refrigerator accounts for 13.5% of the total energy consumption by RHLM using a 460L top-mount refrigerator.

The heat transfer at the door gasket is mainly due to conduction, convection, radiation, and air infiltration into the chamber of refrigerator. In addition, water vapor may also infiltrate, which may cause more energy consumption during the defrost cycle of the freezer.

Pradeep [10] states that a good door seal should “conform to the contour of the surface” and be “compressible and flexible enough to overcome the geometrical tolerance”. For the purpose of reducing the energy consumption of the refrigerator, more attention should be focused on improving the efficiency of the door gasket of the refrigerator. One possible reason for the sparsely available open literature about the energy efficiency of the door gasket is that it is largely dependent on the variations of the cabinet and door designs of different types of refrigerator.

## 1.1 Previous Research on the Heat Loss at the Door Gasket of the Refrigerator

Although open literature about the numerical simulation of the heat loss at the gasket of the refrigerator is sparsely available, there is some representative research work which highlights the progress. In the research of Kim [11], a series of experiments are run under the working condition of the refrigerator with the thermocouples placed at the gasket region to measure the temperature at the inside and outside walls and door and the gap between the door and the gasket. In the corresponding CFD simulation, a constant inlet temperature and assumed convective heat transfer coefficient are used. The limitation of Kim's research is that a constant convective heat transfer coefficient is assumed in the first place, but the convective heat transfer coefficient is unknown under most real circumstances. Similarly, the incoming air is assumed to be uniform and a constant for approximation, however, this assumption lacks experimental validation. Therefore, the accuracy and generality of the results of Kim's research work is limited.

In the research of Huelsz [12], a 3D CAD model is built to simulate the heat transfer at the gasket region. An incompressible laminar flow is assumed to dominate the air flow in the chamber of the refrigerator and the pressure difference inside the chamber is negligibly small. The Boussinesq approximation is used to model the heat transfer mechanism at the door gasket of the refrigerator without the consideration of the effect of radiation.

The air infiltration through the open door of a refrigerated room is simulated by Foster

and Barret [14], with the inlet velocity measured by the hot wire anemometers to provide more accurate boundary conditions for a $k-\varepsilon$ turbulent model. Although the refrigerated room is different than the domestic refrigerator on the aspects of design and operation, however, the pressure difference between the inside chamber and the environment caused by temperature difference is always the main force of air infiltration at the door gasket for both the domestic refrigerator and the refrigerated room.

## 1.2 CFD Simulation of the Airflow within the Chamber of a Refrigerator

As indicated by the EPA [6], the flow field near the door gasket region has more influence on heat transfer than the specific thermal properties of the door gasket than the inside chamber flow field. Therefore, it is of importance to know the flow field in the refrigerator chamber, especially near the gasket region. Hence, the following is going to introduce the flow field within the chamber of the refrigerator in accordance of the two types of domestic refrigerators: static type and ventilated type.

### 1.2.1 Static Type of Refrigerator (without Fan)

A static type of refrigerator is defined as a refrigerator without the electric fan for the purpose of intensifying the cold air flow. Natural convective heat transfer within the chamber of the refrigerator has been investigated by many researchers. Air flow by natural convection in an empty cavity is correlated to the difference of wall temperature. The temperature of the wall with the evaporator is colder compared to the other walls, and this

temperature difference results in natural convective heat transfer and the flow circulation within the chamber of the refrigerator. The flow field is dominated by laminar flow for the static refrigerator [15, 16, 17].

Two types of air circulation exist in the cavity according to the research of Tian and Karayiannis [15]. The first type is the primary air recirculation loop near to the walls, and the second one consists of small recirculation loops located between the boundary layers and the center of the cavity. The Rayleigh number is an important variable in determining the characteristic of the flow field in the static refrigerator chamber. According the literature review of Laguerre [16], Rayleigh numbers range from $10^8$ to $10^9$ in the chamber of a static refrigerator, which further confirms the conclusion that the laminar flow is dominant within the chamber of the static type refrigerator.

The research work of Laguerre [18] and Bayer [19] shows that the heat transfer due to radiation is significant inside the chamber of the refrigerator. The Discrete Ordinate Method (DOM) coupling with the convection model is popularly used among researchers [18, 19, 20] for the purpose of evaluating the effect of radiation heat transfer.

The non-uniformity of the temperature distribution is observed both in experiments and numerical simulations [19, 21, 22]. Laguerre [19] confirms the existence of temperature stratification, which is the fact that the air temperature at the bottom of the chamber is lower than the top area of the refrigerator. Furthermore, the stratification effect

is more obvious when radiation is taken into account. Obvious temperature non-uniformity at the corners of the chamber is observed in CFD simulations as well [22, 23]. According to the research work of Laguerre [19], the temperature is relatively homogeneous at a given height and the air temperatures increase with the increasing numbers of obstacles.

Similarly, Guo and Hong [23] point out that the temperature difference increases with height. The temperature uniformity can be improved if a fan is installed or the difference between the shelves and the walls and door is decreased. If the difference decreases, the flow velocity along the walls will be slower, which results in thicker boundary layers and therefore lower heat transfer coefficient as a result.

In the earlier research of Laguerre [16], the mean thickness of the equivalent thermal layer is estimated by using empirical equations. However, these empirical equations are based on simplified rectangular models, which limits the applications of estimating the thermal layer thickness of real refrigerators. Obtaining the appropriate thickness of the thermal boundary is essential for refining computational meshes near solid-flow boundary, which ensures more accurate simulation results in numerical simulations**.**

### 1.2.2 Ventilated Type of Refrigerator (with Fan)

Sometimes an electric fan is installed inside the chamber of the freezer. Turbulent flow is generated inside the chamber with intensified cooling effect. However, the flow rate of air from the electric fan is “suppressed” for the purpose of preventing freezing,

drying stored food, and extra thermal load obtained from the outside environment. As a result, the temperature is a little higher at the door and upper shelves.

The pattern of turbulent flow is much more complex. Kai and Wen [24] show that by optimizing the design of the fan, the uniformity of the temperature can be better achieved, which can be as much as about 50 % in reduction of the temperature difference. Different turbulence models are used by researchers to investigate the chamber flow field by numerical simulation. Several turbulent models (such as $k-\varepsilon$ model, k-ω model, LRN model, and RSM model, etc.) are detailed discussed in literature review [25] by citing intensive papers. $k-\varepsilon$ model and k-ω model are more frequently used in simulations related to air flow in the chamber of the refrigerator in the most research studies.

## 1.3 Reverse Heat Load Method (RHLM)

The Reverse Heat Loss Method (RHLM) is widely used by researchers [8, 9, 10] to investigate the heat loss or the heat transfer coefficient of the refrigerator. A heating element is placed inside of a non-operating refrigerator and symmetry of the heat transfer is assumed. This method is based on the principle that the energy input to maintain the steady state of the refrigerator equates the heat loss of the refrigerator.

Thermocouples and heat flux sensors are fixed on the surface of the door and walls to measure the temperature and heat flux at different positions of refrigerator. The total energy

input to the system is also recorded with voltage variation dampers [26]. For the purpose of improving accuracy, the steady state should be ensured before any experimental thermal measurements. Some researchers [9, 26] choose to measure after 20 hours to ensure the achievement of steady state. The temperature measured by different thermocouples may vary slightly, but of more interest is the mean temperature. An electric fan can be installed in the chamber of the refrigerator to improve the uniformity of the temperature distribution, however, the exact energy input of the electric fan (which is an external and extra energy input) must be recorded accordingly.

RHLM is more frequently used to obtain the heat transfer coefficient of the door and the walls and the interface between the refrigerator and the freezer. It should be noted that RHLM does not consider the operation of the compressor and the complex geometry of refrigerators as it is a simplified model purely aiming to investigate the general heat transfer mechanism.

## 1.4 The Objectives of the Present Study

The primary objectives of this study are to obtain the effective heat leakage in energy leakage per unit time, per unit length along the gasket, and per degree of temperature difference (eg.W/m·K) across the gasket region of domestic refrigerators, and to be able to distinguish differences in heat leakages between different gaskets. To do so requires

knowing the heat flux rate exiting the gasket region continuously along the surface normal to the gasket. To this end an experimental test cell was constructed which isolates the gasket region. However, only six experimental measurement locations are available. Therefore, CFD is performed to provide "shape profiles" which can be used to best fit the experimental data via a Least Mean Square Error approach. These then provide the continuous heat flux profiles which are then numerically integrated to obtain the desired heat leakage. The CFD is the focus of this thesis. The CFD is also used to investigate the relative changes in heat leakages associated with the freezer section hot loop, forced convection due to the evaporator fan, as well as the effects of including radiation heat transfer in the simulations.

# CHAPTER 2: NATURAL CONVECTION SIMULATION

## 2.1 The Geometry of the Simulation Domain

The CFD simulations are based on a test cell built to investigate the heat loss at the gasket of the domestic refrigerator. The test cell contains a cubic interior of $60\,cm \times 60\,cm \times 60\,cm$ approximately. Based on the principles of RHLM, a heater provides constant heat energy is installed within the interior of the test cell, which is shown in Fig.1. The purpose of the test cell is to measure heat losses through the gasket region in a simplified and controlled environment. Different doors and/or gaskets can easily be inserted into the test cell. The author provided some assistance with the experiments; however, his contributions, and the content of this thesis, are predominantly on the CFD portion of the project.

Based on the test cell built mentioned above, a 3D CAD model is constructed in CATIA V5™ and a 2D middle-surface is extracted and imported into ANSYS Fluent 14.0™. The 2D simulation domain is meant to mimic the symmetric center plane of the experiment and is shown in the following in Figure 2. Note that by being 2D it is not expected that the actual temperatures inside the test cell will be accurately predicted. However, the 2D model should be able to predict the approximate "shape" of the heat flux exiting the measurement surface [see Figs. 1 (b) and 2 (b)]. The ultimate objective is to measure the "effective heat leakage" for each gasket is first obtained as a W/m (per unit length of the gasket region) through numerical integration:

$$W/m = \int (W/m^2)(s)ds. \quad (2.1)$$

For the present report all integration is from s=0 to s=31 cm. This value is then divided by the temperature difference to obtain a heat leakage in units of W/m.K.


(a)

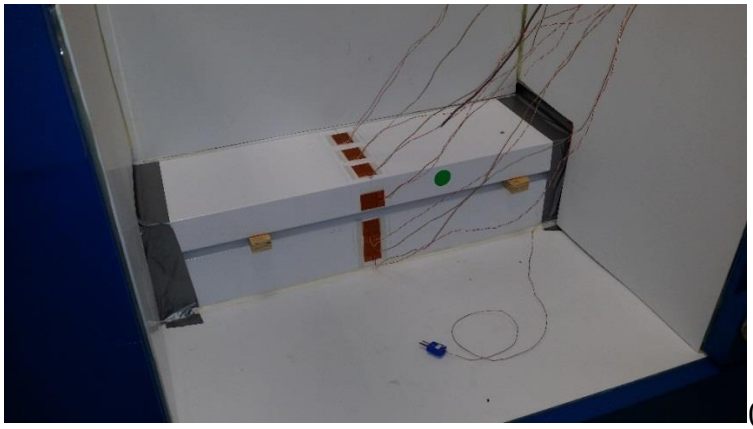
(b)

Figure 1: The (a) test cell interior with the heater inside the chamber, and (b) exposed gasket region with the test cell sealed.

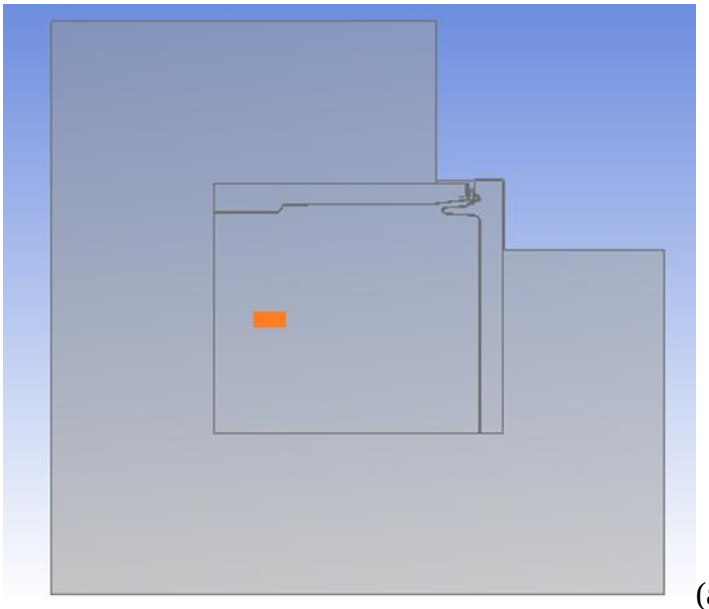

(a)

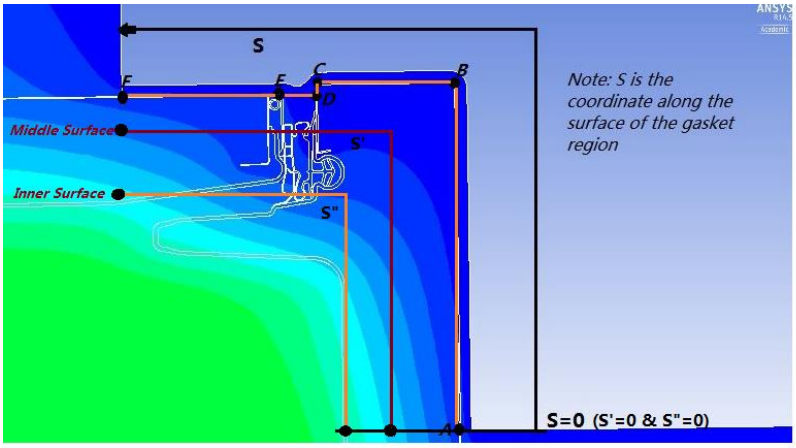


(b)

Figure 2: The (a) 2D simulation domain of the test cell. The orange rectangular indicates the heater, and (b) a zoom in of the 2D CFD domain of interest showing different surface and interior paths for which the heat flux is to be simulated.

As shown in Fig. 2, the test cell is composed of the door panel and the wall of the refrigerator, of whose outer surface is surrounded by insulation materials except for the region of the gasket. The insulation material prevents the heat transfer through other regions (except for the gasket) as much as possible although heat leakage still exists in real

measurement (such as the corners where insulation is poor).

## 2.2 Material Properties used in the Present Study

The thermal properties of the materials used in the present simulations are listed in Table 1.

| Material | Density $(kg/m^3)$ | Specific heat $(J/kg \cdot K)$ | Thermal conductivity $(W/m \cdot K)$ |
|---|---|---|---|
| Insulation material of the blue box | 1840 | 1450 | 0.0272 |
| Liner of the refrigerator | 1840 | 1225.1 | 0.3378 |
| Frame of the refrigerator | 7830 | 650 | 45.2 |
| Magnet | 8000 | 650 | 12.39 |
| Gasket | 1220 | 1600 | 0.15 |
| Foam | 1840 | 1450 | 0.022 |
| Heater (Copper) | 8978 | 381 | 387.6 |
| Air | 1.225 | 1006.4 | 0.0242 |

Table 1: The thermal properties of the materials used in the present numerical simulations.

ANSYS Fluent 14.0™ was chosen to solve the conjugate heat transfer problem and was run in double precision mode to assist in achieving as accurate results as possible [27].

## 2.3 Natural Convection (Boussinesq Model)

In the numerical simulation, the heater is installed in the chamber of the refrigerator, which generates the air flow because of natural convection. Natural convective air flows can be either laminar or turbulent. However, according to the literature review of Lauerre [16], Rayleigh number in the chamber ranges from $10^8$ to $10^9$ in the chamber without air ventilation, which indicates that laminar natural convective flow is dominant.

In the case of the present numerical simulations, natural convective flow arises due to the change of the fluid density because of the temperature change. For natural convection with the Boussinesq approximation, the density change of the flow is relatively small and the flow density is treated as a function of temperature [28].

$$(\rho - \rho_0) \approx -\rho_0 \beta (T - T_0) g \qquad (2.2)$$

In equation (2.1), $\rho_0$ represents the constant density of the flow, $T_0$ represents the operating temperature, and $\beta$ is defined as the expansion coefficient:

$$\beta = -\frac{1}{\rho}\left(\frac{\partial \rho}{\partial T}\right) \qquad (2.3)$$

The governing equations with the Boussinesq approximation can be written as the following:

$$\mathrm{u}\frac{\partial u}{\partial x} + v\frac{\partial u}{\partial y} = -\frac{1}{\rho}\frac{\partial P}{\partial x} + \nu\left(\frac{\partial^2 u}{\partial x^2} + \frac{\partial^2 u}{\partial y^2}\right) \tag{2.4}$$

$$\mathrm{u}\frac{\partial v}{\partial x} + v\frac{\partial v}{\partial y} = -\frac{1}{\rho}\frac{\partial P}{\partial y} + \nu\left(\frac{\partial^2 v}{\partial x^2} + \frac{\partial^2 v}{\partial y^2}\right) + \beta g(T - T_\infty) \tag{2.5}$$

$$\mathrm{u}\frac{\partial T}{\partial x} + v\frac{\partial T}{\partial y} = \left(\frac{k}{\rho C_p}\right)\left(\frac{\partial^2 T}{\partial x^2} + \frac{\partial^2 T}{\partial y^2}\right) \tag{2.6}$$

$$\beta = -\frac{1}{\rho}\left(\frac{\partial \rho}{\partial T}\right) \tag{2.7}$$

## 2.4 Boundary Conditions for Natural Convection Simulation

The primary boundary conditions that needed to be set are the external surface temperatures on the outer perimeter of the geometry, which is shown in Figure 3.

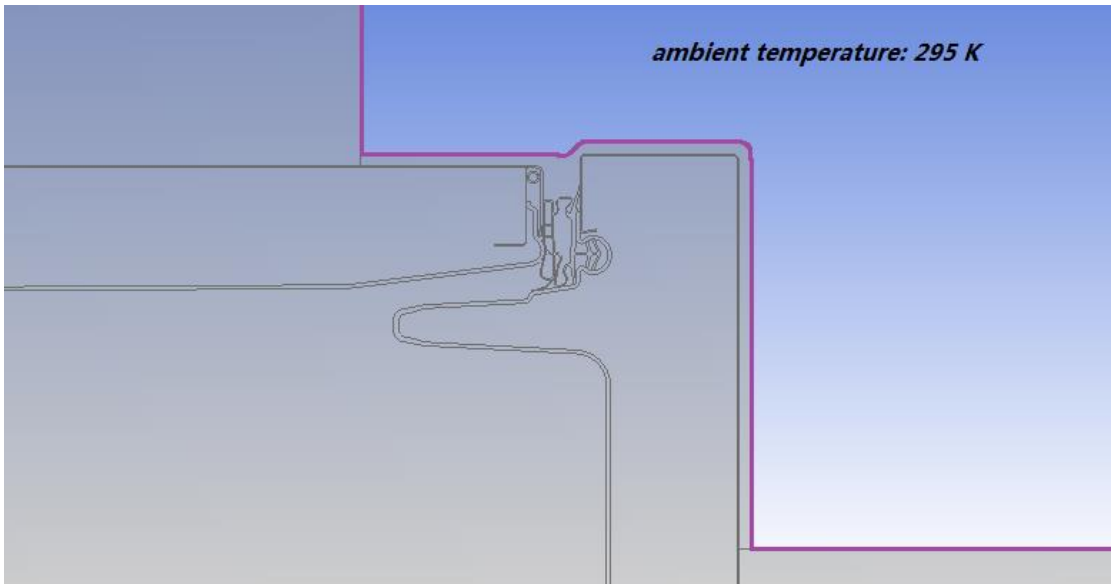

Figure 3: The gasket region of the test cell and the implementation of boundary conditions for natural convection.

The ambient temperature is measured to be 295 K and is assumed to remain constant approximately for the purposes of the CFD. This temperature was the (measured) surface boundary temperature for all exposed insulated surfaces. However, measurements of the gasket region surface temperature showed it to be higher than ambient. Therefore, experimental measurements of the thermal boundary layer were made and it was determined to be approximately 5 mm in thickness. It should be noted that the most accurate thickness of the thermal boundary layer is difficult to calculate by theory, hence, 5 mm thickness of the thermal boundary layer is an estimation based on the experience of temperature measurement. Therefore, the CFD domain extends 5 mm into the surrounding ambient air at which the ambient room temperature boundary condition is applied.

This assumption was tested through a series of initial guesses of the thickness of the

boundary layer are attempted. Numerical simulations are performed by using different thicknesses of thermal layer (e.g. 1 mm, 2 mm, 3 mm and so forth). Then the temperature along the surface of the gasket region under the assumption of different thermal layer thicknesses is compared with the experimental results. It is found that 5 mm thickness of the thermal boundary layer is the most close to the actual experimental results.

The thermal boundary layer is assumed to be quiescent in the present study. All other outer surfaces (insulation material surfaces) are assumed to be at the ambient temperature as confirmed by experimental measurements. The energy input of the heater is added as a source term in the settings of ANSYS Fluent 14.0™, whose value is a constant, by adding it into the governing equations.

## 2.5 Mesh Quality

The accuracy of the CFD simulation heavily depends on the quality of the mesh. The mesh is generated in ANSYS MESH 14.0™ and the mesh at the regions of the gasket, liners, steel frames of the refrigerators are further refined. Orthogonal quality is considered to be the primary criteria in mesh generation and highly skewed cells are avoided where possible. Figure 3 shows an example mesh of the gasket region generated in ANSYS MESH 14.0™. The entire domain shown in Fig. 2 (a) is also meshed to high quality through a series of refinements based on gradients as well as “y+” criteria when using a turbulence

model for forced convection simulations discussed below.

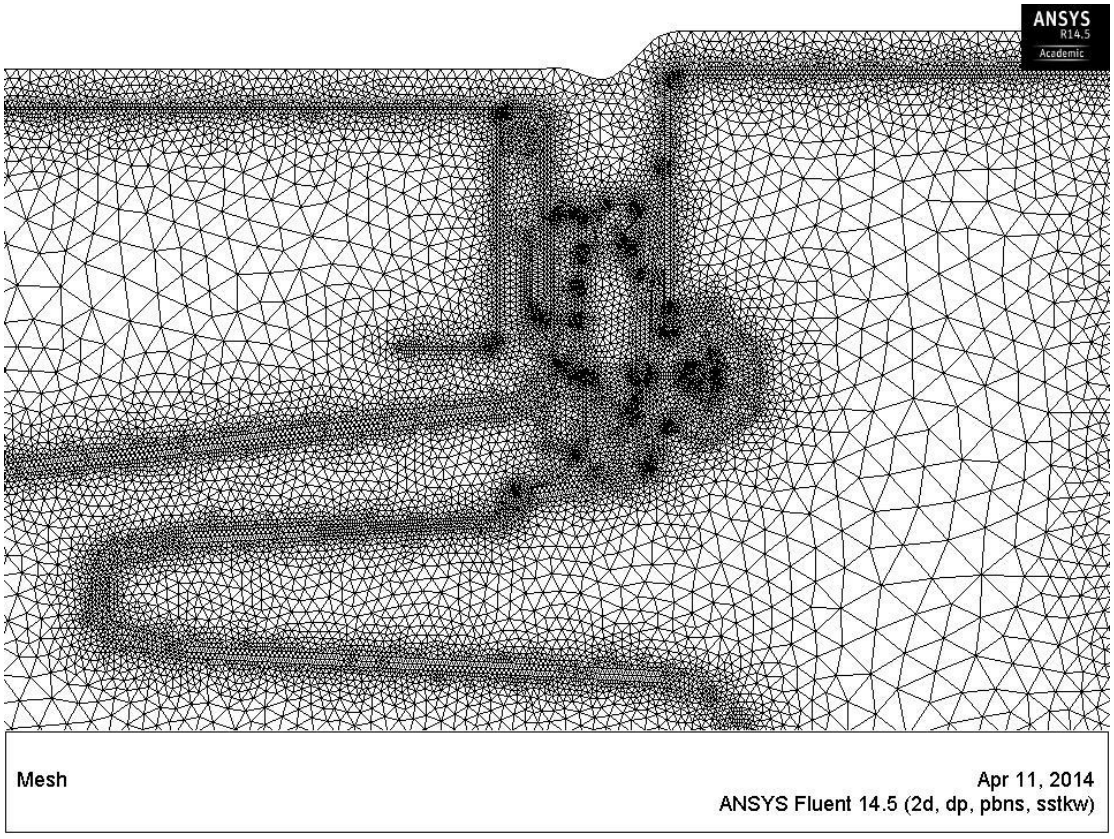


Figure 4: Example mesh of the gasket region generated in ANSYS MESH 14.0.

## 2.6 Convergence Criteria

The convergence of the steady CFD simulations is controlled by monitoring the residuals of the mass, momentum, and energy equations with the number of iterations. Although ANSYS Fluent 14.0™ has default setting values for convergence criteria, these values are too large to be accepted. In the present study, the default settings are lowered

to $10^{-12}$. A more frequently used method for convergence is to monitor a variable to see whether this value changes with further iteration. The temperature derivative normal to the gasket outer surface is monitored with the iterations. The simulation result is considered to achieve converged steady state when the monitored value does not change with iteration. Figure 5 shows an example monitor of the convergence of the CFD simulation.

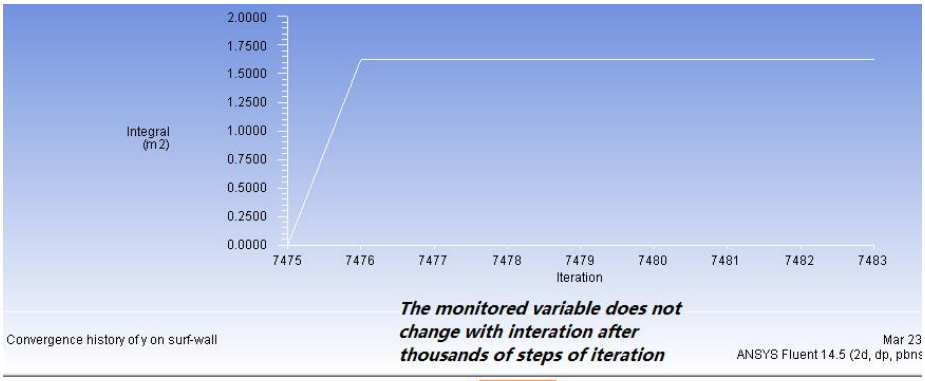


| iter | continuity | x-velocity | y-velocity | energy | surf-mon-1 | time/iter |
|---|---|---|---|---|---|---|
| 7475 | 6.2762e-03 | 2.4445e-04 | 1.7005e-04 | 4.1278e-10 | 0.0000e+00 | 0:00:00 10000 |
| 7476 | 6.3227e-03 | 2.4418e-04 | 1.6950e-04 | 4.1450e-10 | 1.6244e+00 | 5:33:18 9999 |
| 7477 | 6.2571e-03 | 2.4354e-04 | 1.6937e-04 | 4.1382e-10 | 1.6244e+00 | 4:59:56 9998 |
| 7478 | 6.3205e-03 | 2.4323e-04 | 1.6887e-04 | 4.1419e-10 | 1.6244e+00 | 5:06:34 9997 |
| 7479 | 6.2705e-03 | 2.4263e-04 | 1.6874e-04 | 4.1097e-10 | 1.6244e+00 | 5:11:53 9996 |
| 7480 | 6.3197e-03 | 2.4236e-04 | 1.6814e-04 | 4.1143e-10 | 1.6244e+00 | 4:42:48 9995 |
| 7481 | 6.2448e-03 | 2.4177e-04 | 1.6801e-04 | 4.0826e-10 | 1.6244e+00 | 4:52:50 9994 |
| 7482 | 6.2809e-03 | 2.4145e-04 | 1.6730e-04 | 4.0734e-10 | 1.6244e+00 | 5:00:52 9993 |
| 7483 | 6.1963e-03 | 2.4077e-04 | 1.6711e-04 | 4.0455e-10 | 1.6244e+00 | 4:33:59 9992 |

Figure 5: The exemplary of the monitor of the convergence of the CFD simulation.

It should also be noted that the initial mesh generated in ANSYS MESH 14.0™ may be not refined enough to ensure the accuracy of the simulation. Further refinement is needed where necessary by mesh adaptation. Mesh adaptation is created based on gradients of temperature. By comparing the predicted profile of temperature before and after mesh adaptation, it can be determined whether further mesh adaptation is needed. The solution

is considered to be mesh independent if no further changes to the solution occur upon further mesh refinement.

# CHAPTER 3: FORCED CONVECTION SIMULATION

## 3.1 Modification of the Geometry

In the chamber of the freezer compartment of a domestic refrigerator, an electric fan is installed on the back wall of the freezer near the evaporator, whose purpose is mainly providing intensified cooling effect. Several CFD simulations were performed including a modeled fan to predict the relative change in gasket region heat transfer attributed to the forced convection. Because of the inclusion of the electric fan, the geometry of the domain is modified accordingly. The simulation domain is symmetric and the modified geometry is show in Figure 6. Note that this is the geometry of an actual refrigerator rather than the test cell for these simulations.

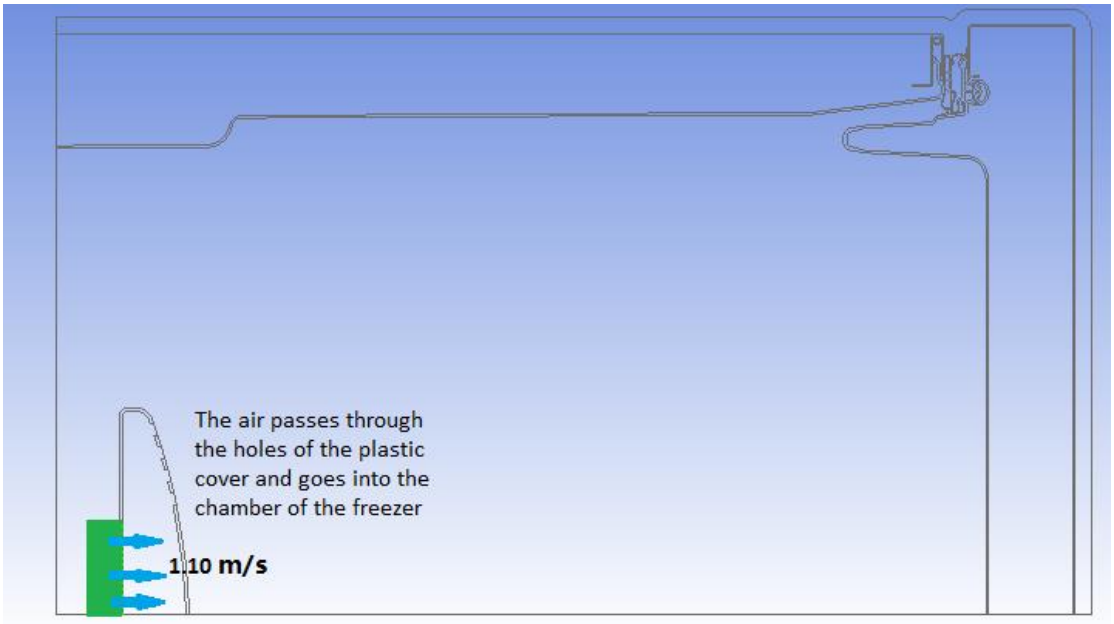


Figure 6: The geometry modification with the electric fan installed. The mean velocity of

the air coming out of the electric fan is measured to be 1.1 m/s by using a hot wire anemometer.

## 3.2 The Choice and Application of Turbulence Models

With the electric fan in the chamber, the airflow is apparently turbulent, hence, the choice of appropriate turbulent models is important for the purpose of accurate simulation. Two of the most widely and frequently used turbulent models for industrial flows are the $k-\varepsilon$ model and $k-\omega$ model.

$k-\varepsilon$ model is a two-equation that solves for the turbulent velocity and length scales independently. The k-epsilon model is the simplest turbulence model and has been applied in practical engineering flows since being proposed by Launder and Spalding [29]. The model includes two equations to represent two turbulence variables, the average turbulence kinetic energy (k) and the average turbulence dissipation ($\varepsilon$). The $k-\varepsilon$ model is easy to converge compared to other turbulence models and can predict many flows. It is commonly used in free-shear layer flows with small pressure gradients and in confined flows where the Reynolds shear stress is of importance. But it does not give good prediction of swirling, rotating flows, and flows with strong separation. It does not predict well in unconfined flow and flows with curvature [30, 31].

Modified $k-\varepsilon$ models are developed to overcome the disadvantages of the standard $k-\varepsilon$ model. Two examples available in ANSYS Fluent are the RNG $k-\varepsilon$ epsilon model and the Realisable $k-\varepsilon$ model. The RNG $k-\varepsilon$ is an improved $k-\varepsilon$

model that can more accurately predict reversed flow and flow separation, wall heat transfer and time dependent flow. The Realisable $k-\varepsilon$ model performs well in flow with jets, rotation, and strong streamline curvature [32].

Similarly to the $k-\varepsilon$ model, the $k-\omega$ model is a two equation eddy viscosity model, which includes two equations to model transported variables: average turbulence kinetic energy $(k)$ and average specific dissipation $(\omega)$. $k-\omega$ performs well in capturing flow characteristics in adverse gradients and separating flows. The $k-\omega$ model may produce larger turbulent levels in regions with large normal strain, but less significant than the turbulent level produced in standard $k-\varepsilon$ model. The $k-\omega$ models falls into the category of Low Re-turbulence models so it solves down to the viscous sub-layer [30].

The $k-\omega$ model is a family of models. The most commonly used $k-\omega$ models are the Wilcox $k-\omega$ model, the Wilcox $k-\omega$ modified model and the Shear Stress Transport (SST) model. The SST model is a blend of the $k-\varepsilon$ model and $k-\omega$ model, which is robust and gives good prediction near solid boundaries. It can also better capture the recirculation regions compared with other turbulence models. The SST model uses enhanced wall functions, which requires that the "y+" values of the first grid points nearest any walls reside within $y+ <1$ (y+, pronounced "y plus", being a non-dimensional distance from the wall which is further discussed below). In this region a linear wall

function and the boundary layer profile can be determined to predict the heat transfer between the wall and the fluid. It is also a reliable model for flow separation [31, 33].

For this work the SST two-equation model is chosen for turbulent flow simulations due to its accuracy in predicting surface heat transfer relative to other available models. The kinematic eddy viscosity, turbulence kinetic energy and specific dissipation rate are incorporated in the following equations [34]:

$$\frac{\partial(\rho k)}{\partial t} + \frac{\partial\left(\rho u_j k\right)}{\partial x_j} = P - \beta\rho\omega k + \frac{\partial}{\partial x_j}\left[(\mu + \sigma_k \mu_t)\frac{\partial k}{\partial x_j}\right] \tag{3.1}$$

$$\frac{\partial(\rho\omega)}{\partial t} + \frac{\partial\left(\rho u_j \omega\right)}{\partial x_j}$$

$$= \frac{\gamma}{v_t} P - \beta\rho\omega^2 + \frac{\partial}{\partial x_j}\left[(\mu + \sigma_\omega \mu_t)\frac{\partial \omega}{\partial x_j}\right]$$

$$+ 2(1 - F_1)\frac{\rho\sigma_{\omega 2}}{\omega}\frac{\partial k}{\partial x_j}\frac{\partial \omega}{\partial x_j} \tag{3.2}$$

In equation (3.2),

$$P = \tau_{ij}\frac{\partial u_i}{\partial x_j} \tag{3.3}$$

$$\tau_{ij} = \mu_t\left(2S_{ij} - \frac{2}{3}\frac{\partial u_k}{\partial x_k}\delta_{ij}\right) - \frac{2}{3}\rho k\delta_{ij} \tag{3.4}$$

$$S_{ij} = \frac{1}{2}\left(\frac{\partial u_i}{\partial x_j} + \frac{\partial u_j}{\partial x_i}\right) \tag{3.5}$$

## 3.3 Boundary Conditions for Forced Convection

The velocity of the fan is designated as an inlet velocity, which is measured to be 1.a m/s by the hot wire anemometer in the lab. For the present study, the air flow before entering into the electric fan is assumed to be a fully developed internal pipe flow with the assumption that the turbulence intensity $(I)$ is 5%. The turbulence kinetic energy is calculated following [27]:

$$\mathrm{k} = \frac{3}{2}(uI)^2 = \frac{3}{2}(1.1 \times 0.05)^2 = 4.54 * 10^{-3} m^2/s^2 \qquad (3.6)$$

The specific dissipation rate $(\omega)$ is calculated as [27]:

$$\omega = \frac{k^{\frac{1}{2}}}{Cu^{\frac{1}{4}} * l} = \frac{(4.54 \times 10^{-3})^{\frac{1}{2}}}{0.09^{\frac{1}{4}} * 0.01} = 12.29/s \qquad (3.7)$$

In Eq. (3.7), the value of $Cu$ is 0.09, which is an empirical constant, and $l$ is a characteristic turbulence length scale which is designated as the fan diameter.

## 3.4 $Y^+$ Values

The viscosity dominant regions with large variable-gradients (such as the bounded walls) have significant influence on the accuracy of turbulent flow simulations. In the present study, the near wall regions need to be carefully modeled to fully capture the turbulent characteristics as the heat transfer is significant at the door/walls of a refrigerator as well as within the test cell. In order to ensure the accuracy of the turbulent characteristics at near wall regions, y+ values need to fall into a certain range as required by the nature of

different types of turbulence models and wall treatments. y+ is a dimensionless wall normal distance defined as:

$$y+= \frac{u_* y}{\gamma} \tag{3.8}$$

In Eq. (3.8) $u_*$ represents the dimensionless friction velocity, $y$ represents the distance to the wall, and $\gamma$ represents the kinematic viscosity of the fluid.

The SST model uses enhanced wall functions (aka the two layer model), which requires the y+ values be < 1. As the small y+ value uses a linear wall function the boundary layer profile can be determined to predict the heat transfer between the wall and the fluid. The viscous sub-layer needs to be fully resolved as the heat transfer at the door/walls is of particular interest. Therefore, it is more appropriate to use a low-Reynolds number turbulence model in this region. This is exactly what the SST model does, making it a good choice for the present application [35, 36, 37]. The surfaces of the wall and the door of the test cell are shown in Figure 7.

In order to limit the y+ values for the SST model, the thickness of the inflation layers at the wall needs to be carefully considered. Based on ANSYS Fluent14.0™ tutorial [27], 10-15 inflation layers are suggested. The thickness of the first inflation layer can be specifically set in ANSYS Fluent 14.0™.

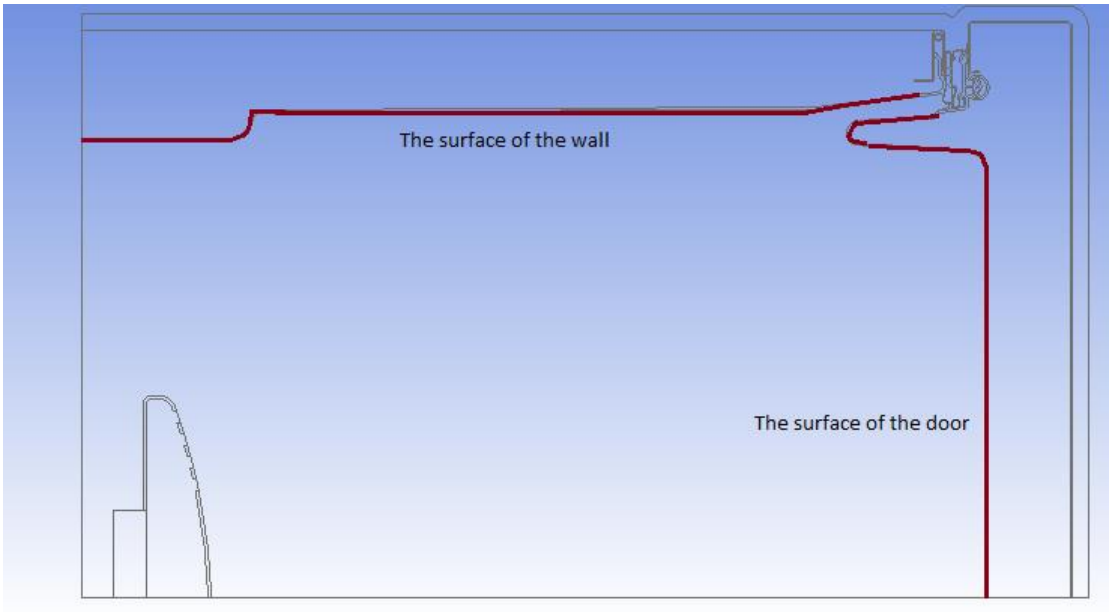


Figure 7: The surfaces of the wall and the door of the freezer.

## CHAPTER 4: RADIATION HEAT TRANFER SIMULATION

With the heater installed in the test cell chamber, radiation heat transfer may also contribute to the total heat loss at the gasket region. In order to estimate the contribution of radiation heat transfer, simulations that incorporated radiation models are also carried out to evaluate the heat transfer increase when radiation is taken into consideration.

In the simulation, the contribution of radiation heat transfer largely depends on the emissivity of the objects, which include the walls and doors of the refrigerator (test cell) and other wooden boards and the chosen radiation model. The emissivity of objects are determined by the properties of the materials, the emissivity of the materials of the test cell is determined to be approximately 0.95 by using a thermal imaging camera, which is shown in Fig. 8.

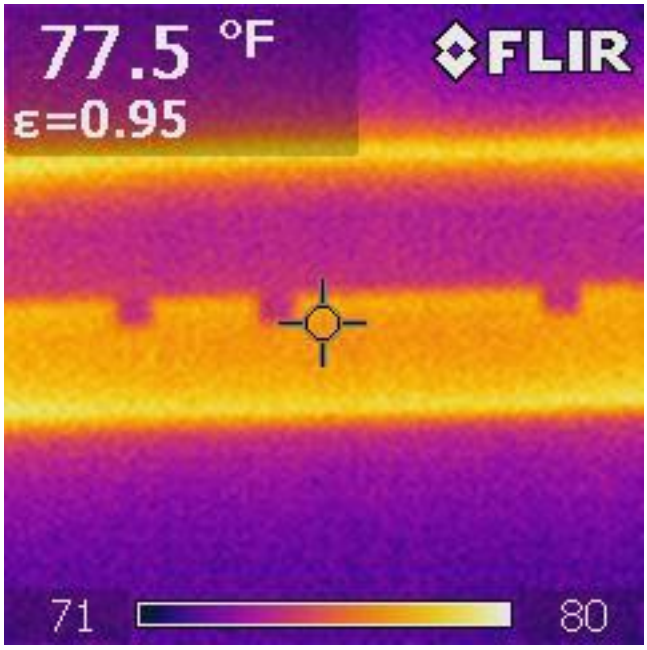


Figure 8: The measurement of the emissivity of the test cell with a thermal imaging camera.

Four different radiation models are provided in ANSYS Fluent 14.0™: the Discrete Ordinates Model (DOM), the Discrete Transfer Radiation Model (DTRM), the P-1 Radiation Model, and the Rosseland Model. The radiation model used in the simulation is the DOM as it can better predict the heat transfer when a heat source is present [1]. The fundamental assumption of the DOM method is modeling the radiative heat transfer leaving the surface with a finite number of discrete solid angles [27].

The equation of DOM radiative heat transfer theory is shown in the following:

$$\frac{\partial I_{si}}{\partial x_i} + (a + \sigma_s) I(r, s) = an^2 \frac{\sigma T^4}{4\pi} + \frac{\sigma_s}{4\pi} \int_0^{4\pi} I(r, s') \Phi(s, s') \, d\Omega' \qquad (4.1)$$

For the purpose of approximation, no scattering effect is considered in the present simulation of radiative heat transfer. Radiation is assumed to occur predominantly between the walls, the door and the heater surface within the chamber of the test cell.

## CHAPTER 5: THE MODELING OF THE HOT PIPE

The hot pipe is an important component in the freezer. It is a portion of the "hot" side of the refrigerant which is looped around the magnetic seals of the freezer chamber. Its purpose is to keep the freezer door seal surface above the dew point temperature so that condensation (and potential freezing) does not occur. The material of the hot pipe is usually metal (aluminum or steel) for assisting the quick and effective release of heat for dew prevention. It should be noted that the hot pipe is not on all the time. As mentioned above, the high temperature liquid is from the compressor, hence, the hot pipe is on only when the compressor is on. Figure 9 shows the location and shape of the hot pipe near the gasket region of the refrigerator.

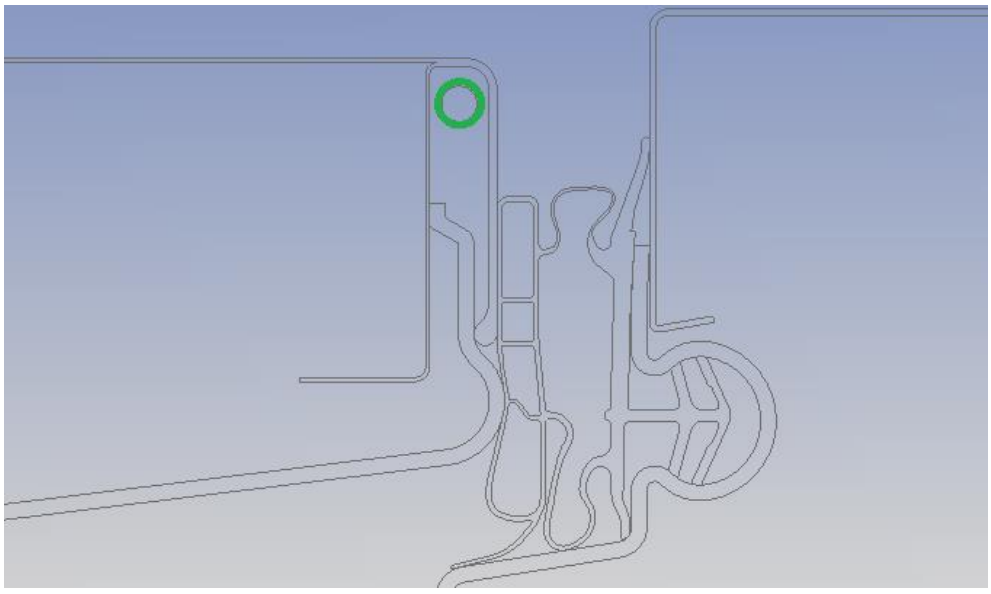

Figure 9: The zoomed in hot pipe (green circle) at the gasket region of the refrigerator.

## CHAPTER 6: DIFFERENT TYPES OF GASKETS USED

For the purpose of making more generalized conclusions, simulations of three different types of gaskets are carried out. Figure 8 shows the geometry of the three types of door gaskets used in the present study. The original CAD model is modified based on the geometries of the gaskets in Fig. 10. The new extracted 2D surfaces are imported into ANSYS Fluent 14.0™ accordingly.

Gasket 1 (Original) Gasket 2 Gasket 3

Figure 10: Three types of door gaskets used in simulations.

# CHAPTER 7: RESULTS AND DISSCUSSION

## 7.1 Simulation Results of Natural Convection with Heat Load of 9.2 W and 15.0 W

In the present study, the temperature of the ambient environment is assumed constant at 295 K. The simulation results of different sets of simulations are presented in Table 2.

| Heat Load | Electric Fan | Model | Heat Leakage |
|---|---|---|---|
| 9.2 W | No | Natural Convection | 0.152 W/m·K |
| 15.0 W | No | Natural Convection | 0.159 W/m·K |

Table 2: Simulated heat leakage for two different heat loads showing the linearity of the heat leakage with temperature difference.

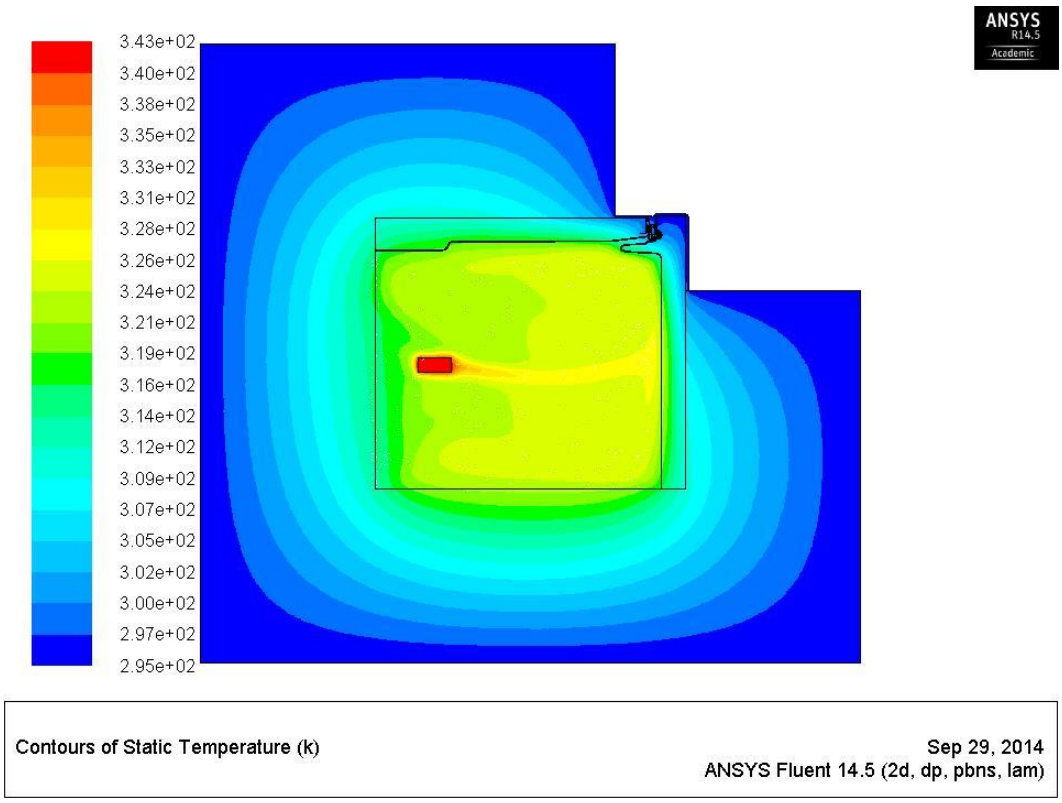


Figure 11: The temperature contour of natural convection with 9.2 W heater energy supply.

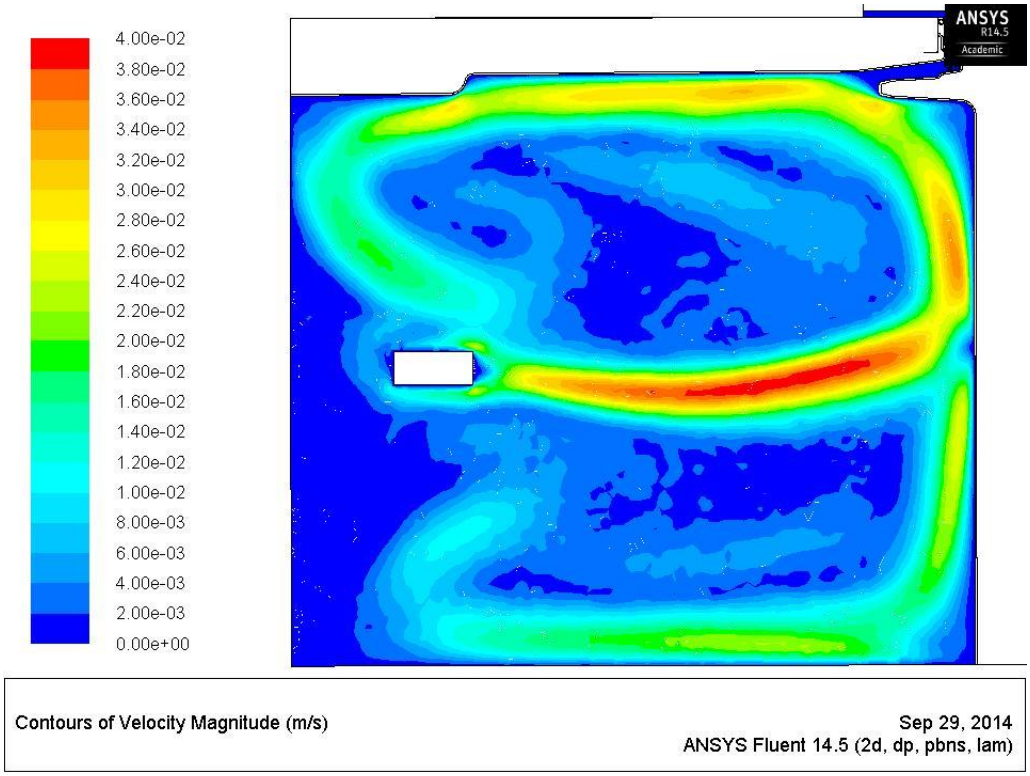


Figure 12: The velocity contour of natural convection 9.2 W heater energy supply.

Table 2 shows the simulated heat leakages for two different heater powers. If the heat leakage in dimensions of W/m·K is independent of the measured temperature difference then this value will be independent of the heat load. The results in Table 2 confirm this linearity, which greatly simplifies the quantification of heat leakages through the gasket region.

As shown from Fig. 12, the air circulation exists within the chamber of the refrigerator. A hot air plume is generated because of natural convection introduced by the heater installed. The flow pattern generally confirms the research results from Karayiannis [15] that the air recirculation exists near the wall in the chamber of the domestic refrigerator.

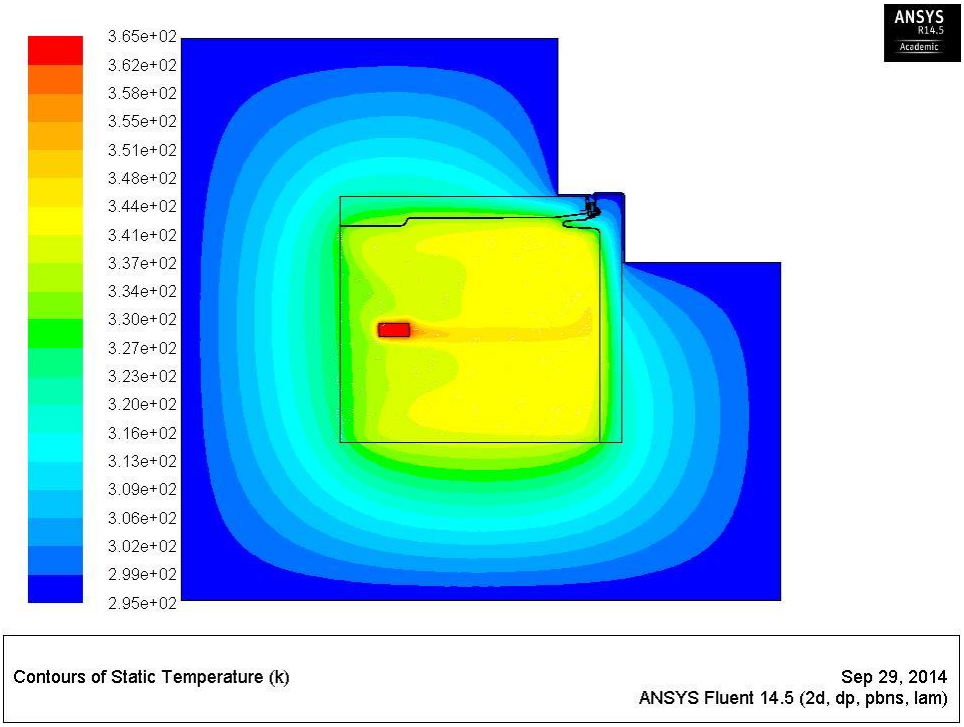


Figure 13: The temperature contour of natural convection with 15 W heater energy supply.

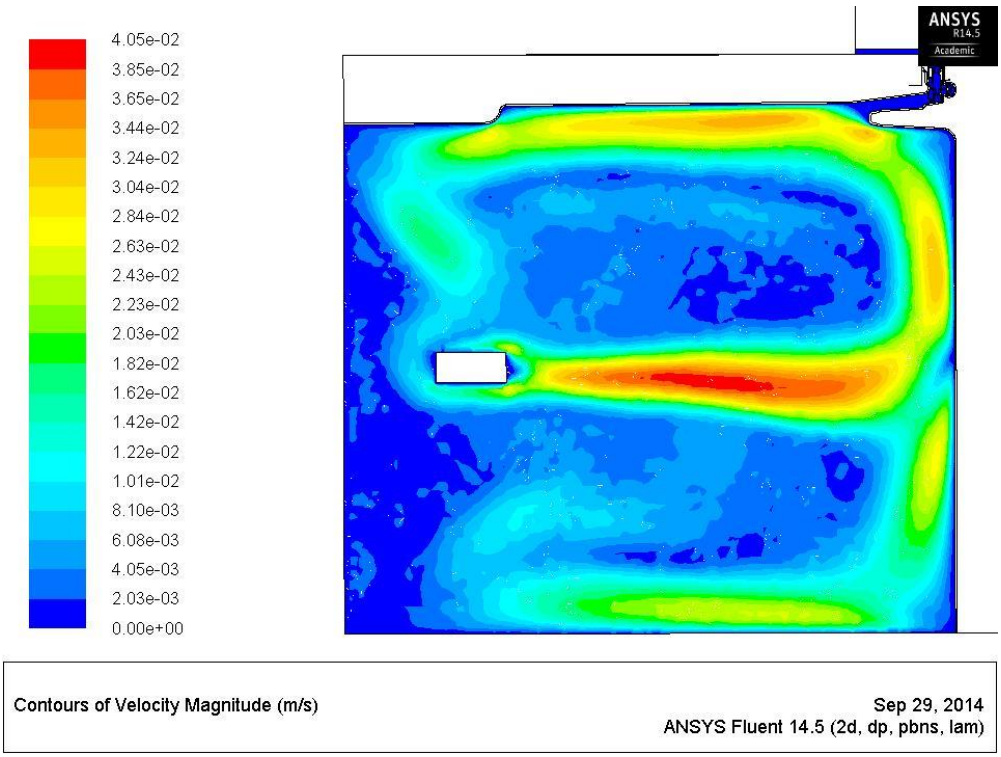


Figure 14: The velocity contour of natural convection with 15 W heater energy supply.

## 7.2 Simulation Results of Forced Convection with 9.2 W Heat Load

| Heat Load | Electric Fan | Model | Heat Leakage |
|---|---|---|---|
| 9.20 W | No | Natural Convection | 0.152 W/mike |
| 9.20 W | Yes | K-ω (SST) | 0.184 W/m·K |

Table 3: Effect of the electric fan on the heat leakage through the gasket region.

From Table 3, the heat loss at the gasket is estimated to increase approximately 21 % when the electric fan is on based on the simulations of the test cell.

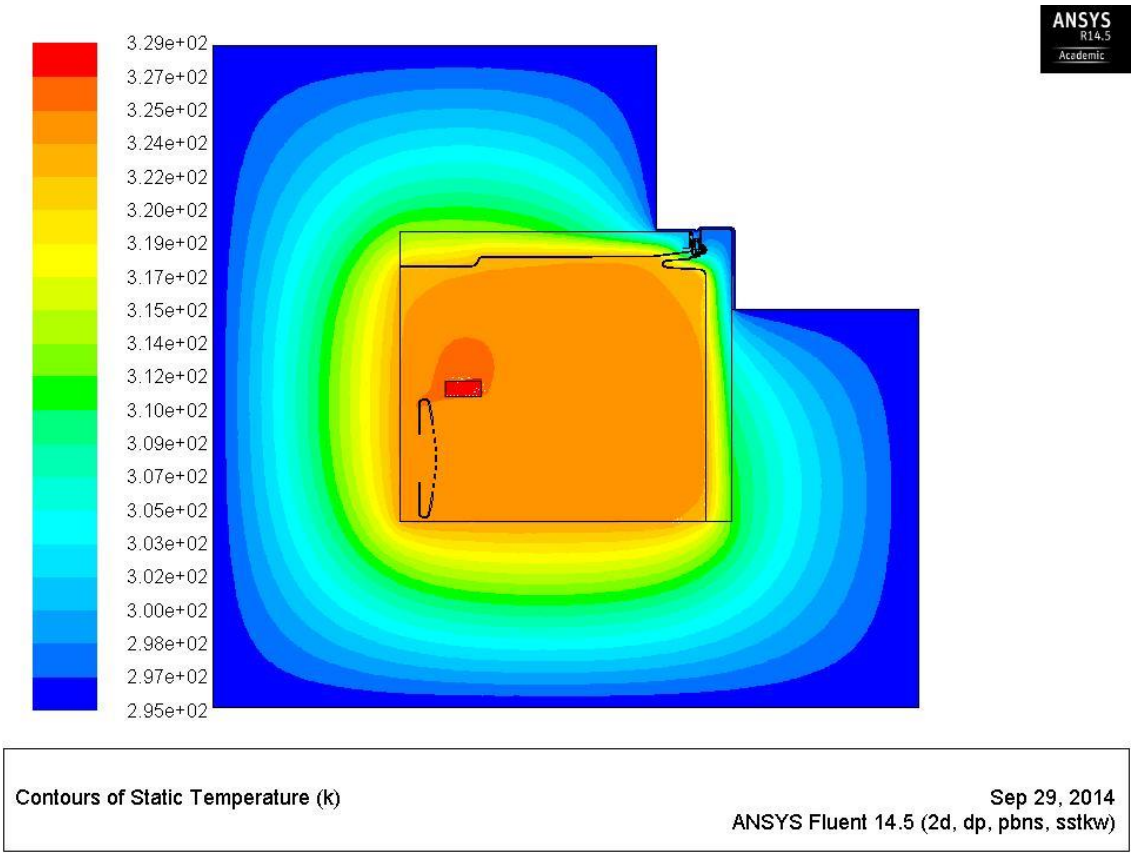


Figure 15: The temperature contour forced convection with 9.2 W heater energy supply.

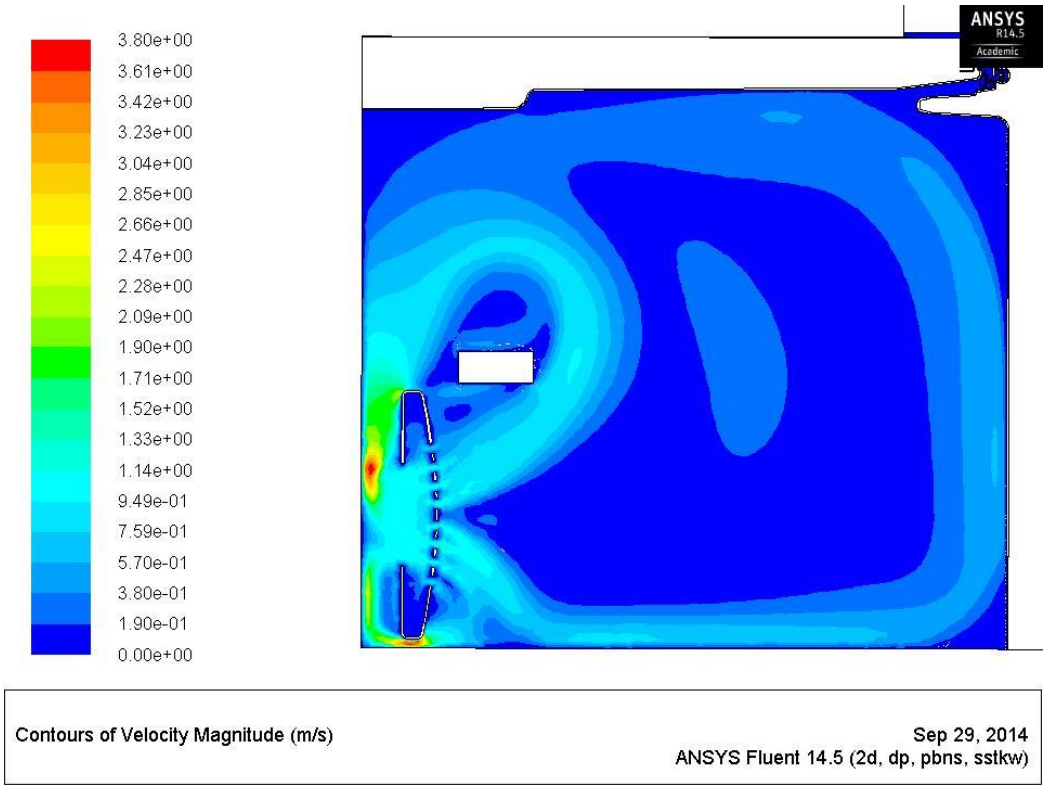


Figure 16: The velocity contour of forced convection with 9.2 W heater energy supply.

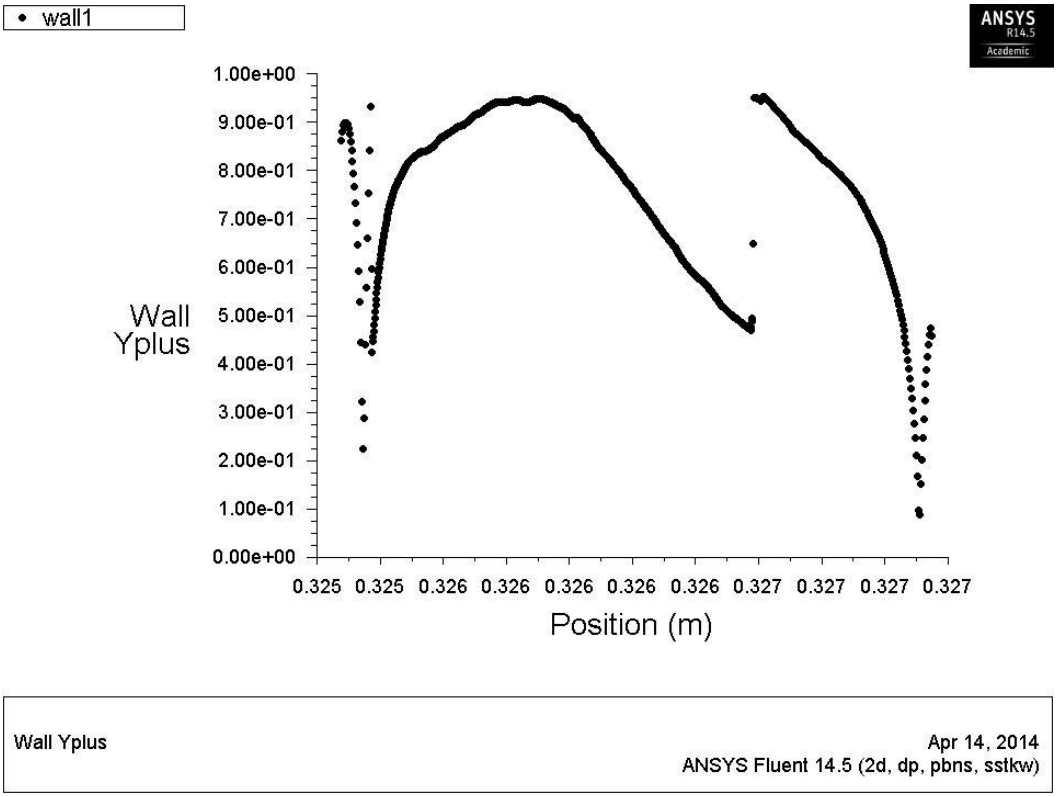


Figure 17: The plot of *y+* values of the wall with 9.2 W heater power.

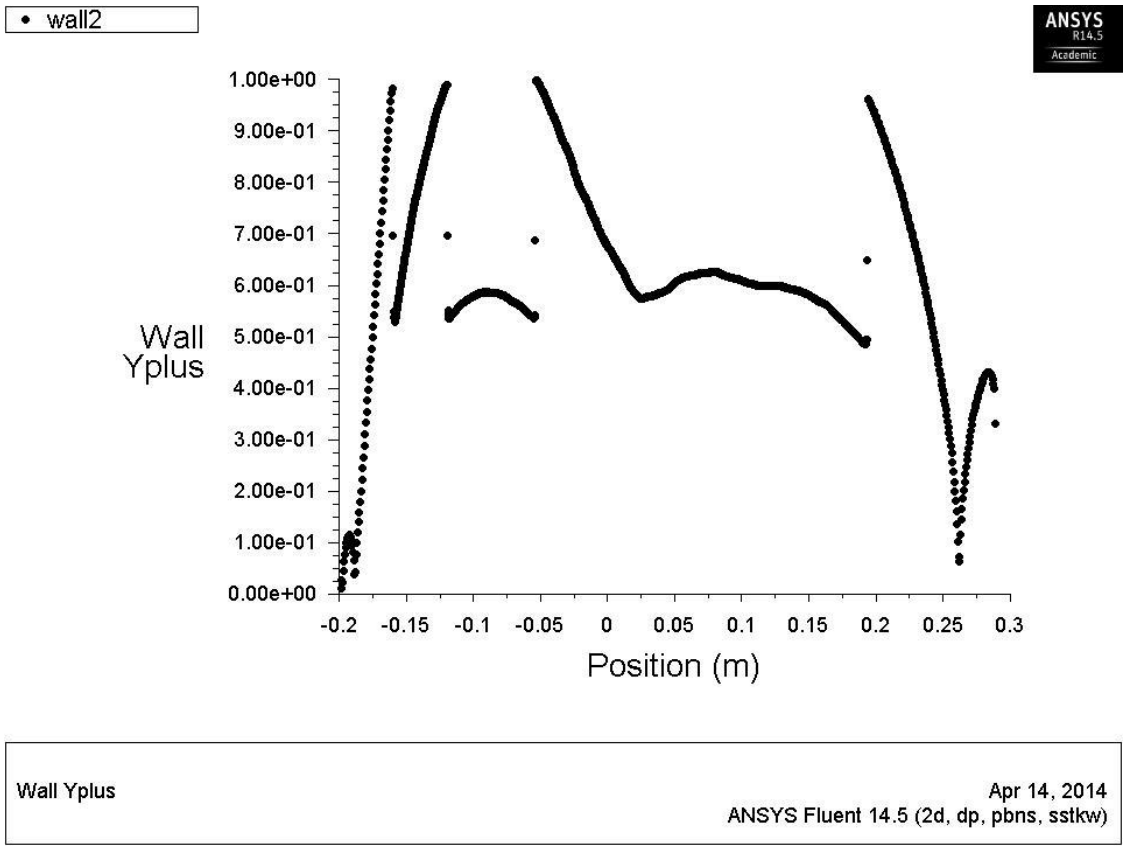


Figure 18: The plot of *y+* values of the door with 9.2 W heater energy power.

From Figs. 17 and 18 it is observed that y+ values at the door and the wall are limited to within 1, however, y+ values are not continuous along the surface. This is due to the presence of adverse flow near the corners and curved edges.

## 7.3 Simulation Results Including Radiation Heat Transfer with the Discrete Ordinate Method (DOM)

| Heat Load | Electric Fan | Radiation Model | Heat Leakage |
|---|---|---|---|
| 9.20 W | No | None | 0.152 W/m·K |
| 9.20 W | No | DOM method | 0.167 W/m·K |

Table 4: Comparison of the heat loss at the gasket between under the conditions of natural convection and radiation heat transfer.

From Table 4, it is shown that the heat loss at the gasket increases around 11 % when radiation is considered. In the present simulation, the radiation model is simplifed and approximated, which is under the assumption of no scattering effect and uniform emissivity.

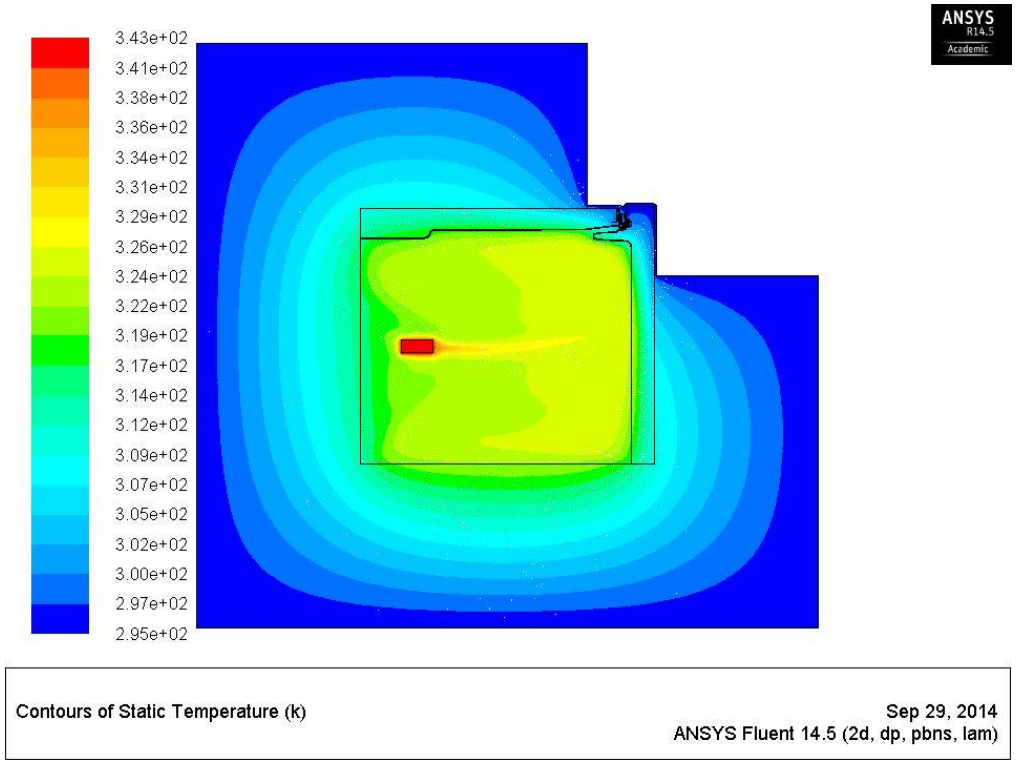


Figure 19: The temperature contour of natural convection with 9.2 W heater energy supply (including the DOM radiation heater transfer model).

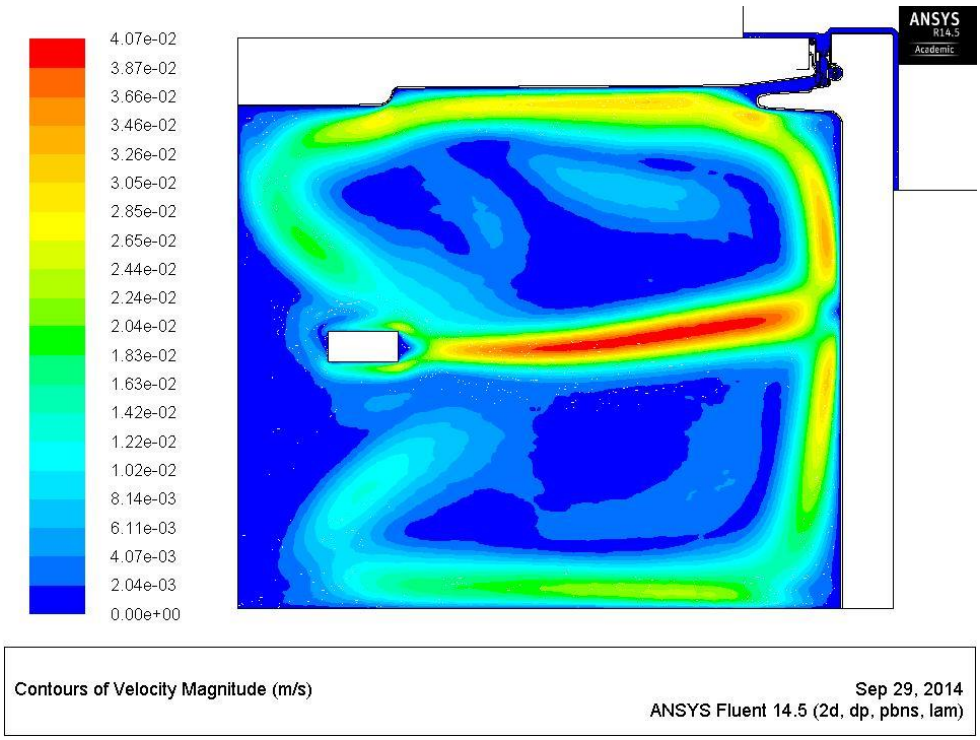


Figure 20: The velocity contour of natural convection with 9.2 W heater energy supply (including the DOM radiation heat transfer model).

## 7.4 Simulation Results of the Heat Loss for Gaskets 2 and 3 under the Condition of Natural Convection

| Heat Load | Gasket Type | Model | Heat Leakage |
|---|---|---|---|
| 9.20 W | Original (Gasket 1) | Natural Convection | 0.152 W/m·K |
| 9.20 W | Gasket 2 | Natural Convection | 0. 184 W/m·K |
| 9.2 W | Gasket 3 | Natural Convection | 0. 176 W/m·K |

Table 5: The comparison of the heat loss at the gaskets between different types of gaskets used in the simulations.

From Table 5 it can be noticed that the original gasket has the least heat loss while

Gasket B has the most heat leakage. It is possibly because Gasket B has a relatively larger hollow cavity at the center of the gasket (shown in Fig. 8), and the hollow cavity allows intensified convective heat transfer within. Hence, one possible solution to reduce the heat loss at the gasket is dividing the hollow portion by multiple small zones to minimize convection within the door gasket. Figures 21 – 26 show the temperature contours corresponding to the three gasket simulations for the test cell geometry. The simulated heat flux profiles along the gasket region are used below in conjunction with experimental measurements.

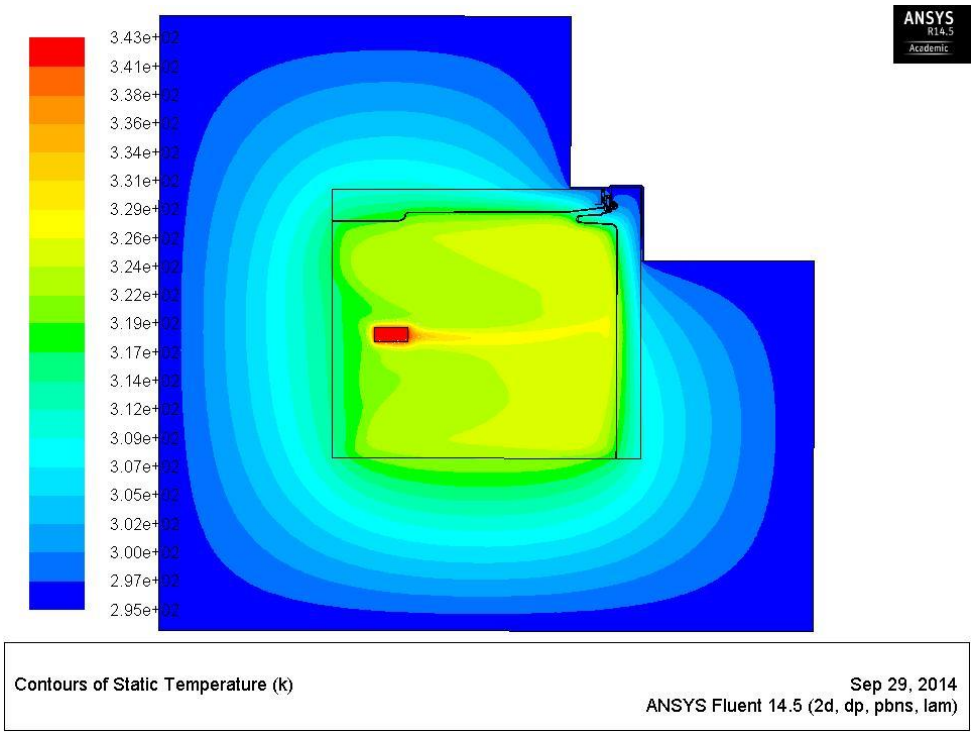


Figure 21: The temperature contour of natural convection with 9.2 W heater energy supply (Gasket 2).

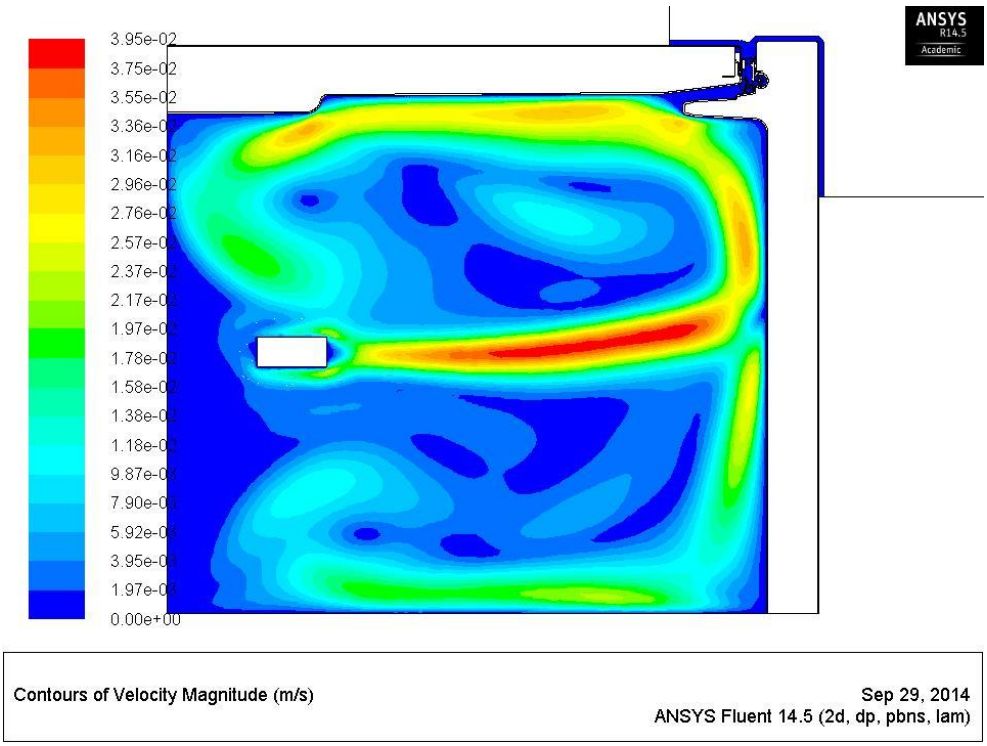


Figure 22: The velocity contour of natural convection with 9.2 W heater energy supply (Gasket 1).

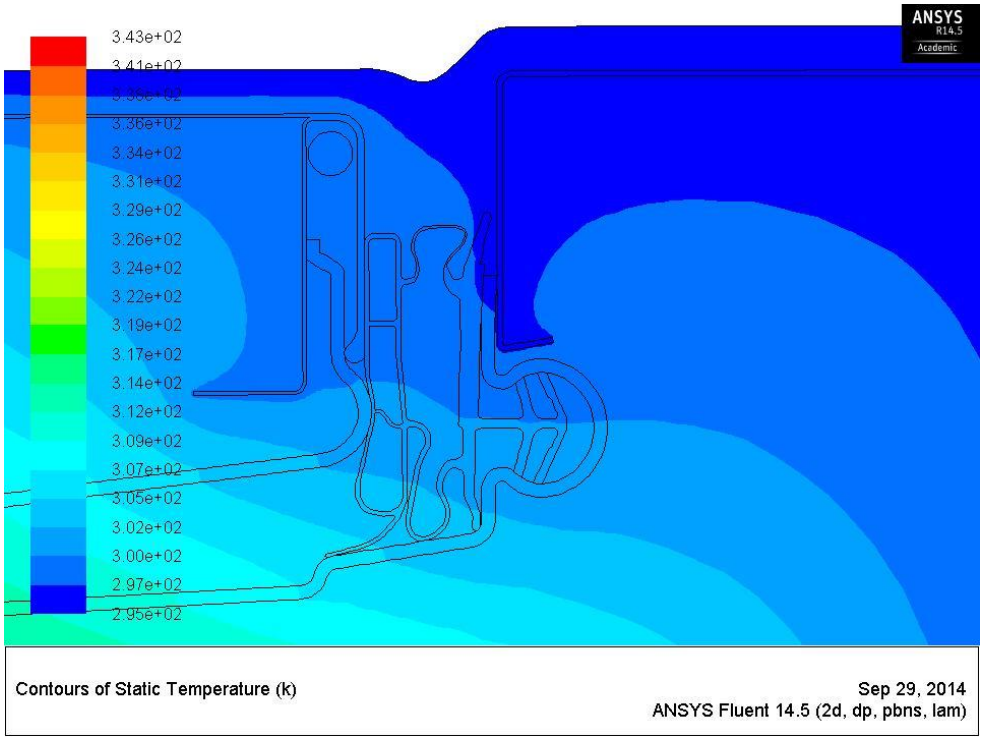


Figure 23: The zoomed in temperature contour of Gasket 2 with natural convection, 9.2 W heater energy supply.

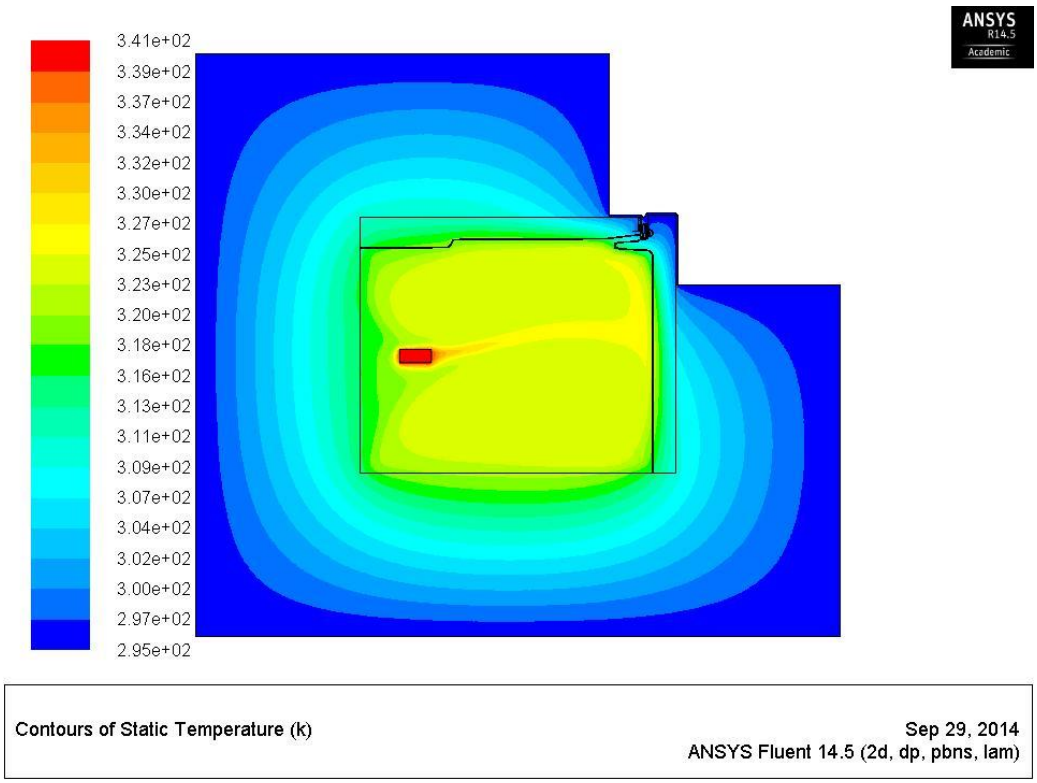


Figure 24: The temperature contour of natural convection with 9.2 W heater energy supply (Gasket 3).

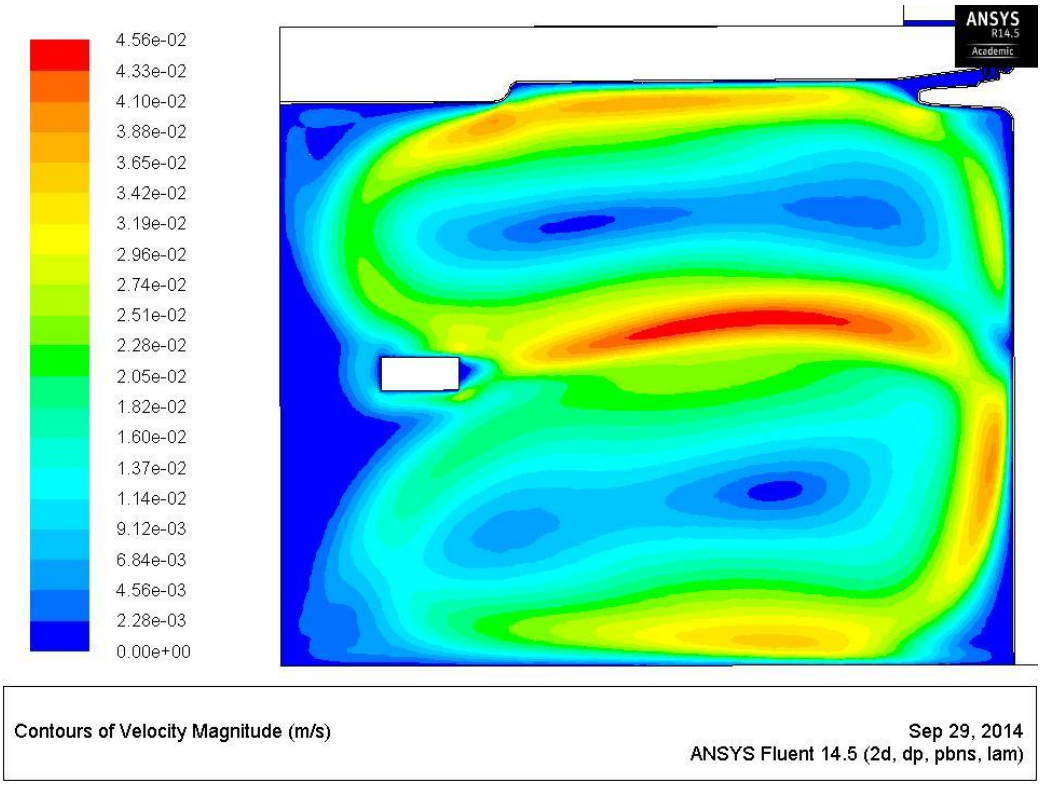


Figure 25: The velocity contour of natural convection with 9.2 W heater energy supply (Gasket 3).

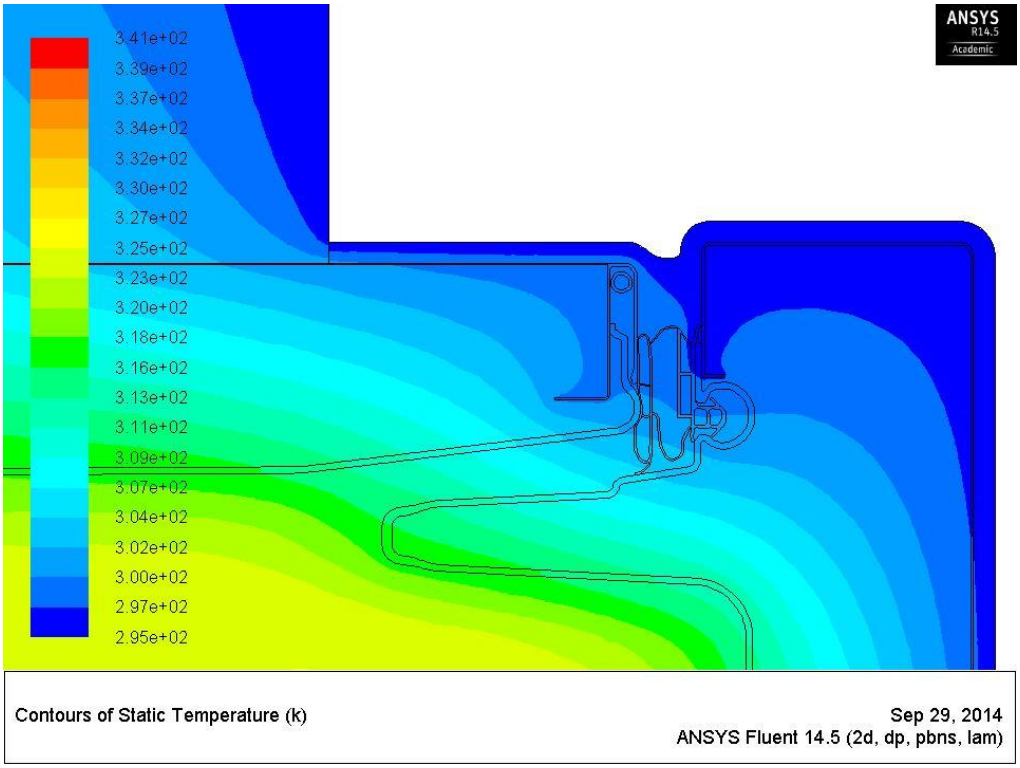


Figure 26: The zoomed in temperature contour of Gasket 3 with natural convection, 9.2 W heater energy supply.

## 7.5 Simulation Results of a Hot Pipe in the Test Cell

Unlike previous simulatons, the investigation of the effect of the hot pipe needs to be conducted under the working conditions of the freezer compartment. Hence, boundary conditions are modified accordingly. The cold air blowing out of the electric fan is set to be a constant temperature of 295 K and the heater is removed from the test cell as there is no need to involve RHLM in the simulaton. The temperature difference between the freezer chamber and the ambient environment is kept 36 K generally. The temprature of the hot pipe is set to be 311 K to mimic the working condition of most domestic refrigeators. The

simulations are based on orginal gasket only. The comparison of the heat loss at the gasket between the simulations with the hot pipe on and off are presented in Table6.

| Hot Pipe | Model | Heat Leakage |
|---|---|---|
| On | Natural Convection | 0.198 W/m·K |
| Off | Natural Convection | 0. 167 W/m·K |

Table 6: The comparison of the heat leakage at the gasket between the simulations with the hot pipe on and off.

As shown in Table 6, the heat leakage at the gasket increases approximately 18 % when the hot pipe is on. Acturally, the heat is emited from the hot pipe as the temperature of the liquid in the hot pipe is higher than the enviroment, whose heat transfer direction is the opposite compared with the rest part of the gasket, the absolute values of the heat that emits outward the hot pipe should be added into the total heat loss of the gasket. Corresponding temperature profiles are shown in Figs. 27 – 30.

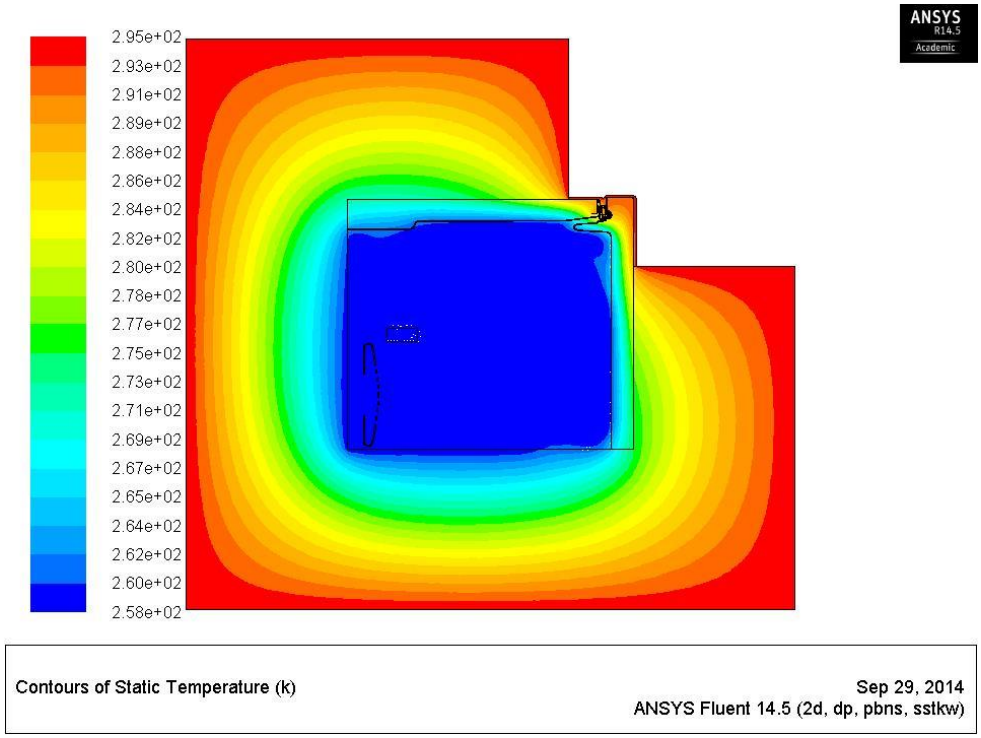


Figure 27: The temperature contour of the test cell with the hot pipe off.

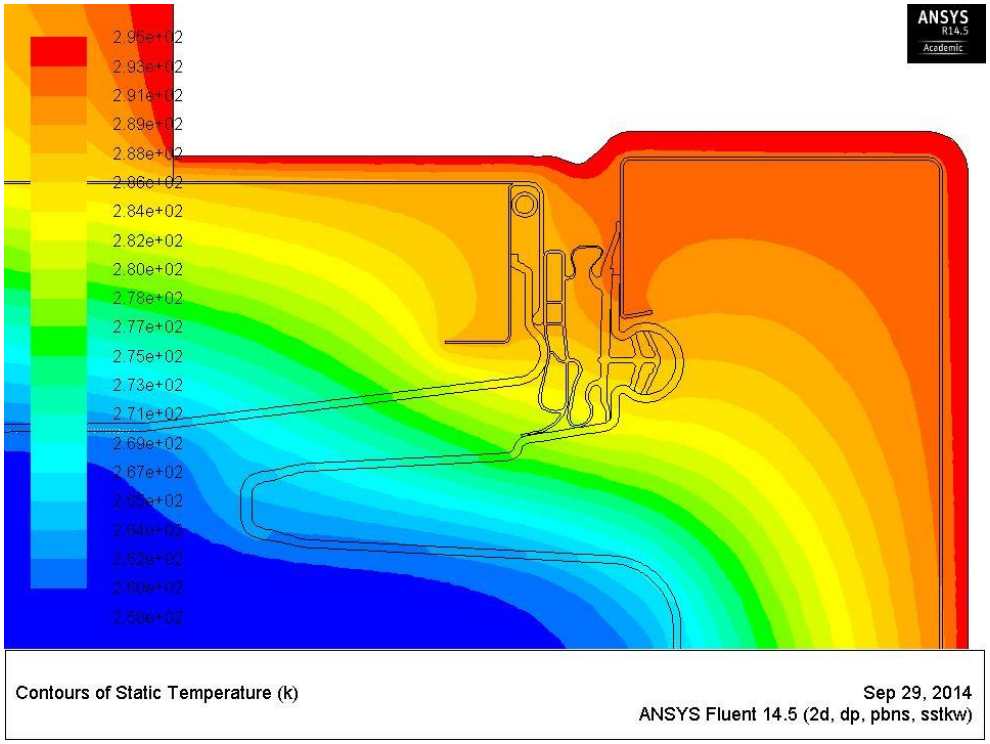


Figure 28: The zoomed in temperature contour at the gasket region with the hot pipe off.

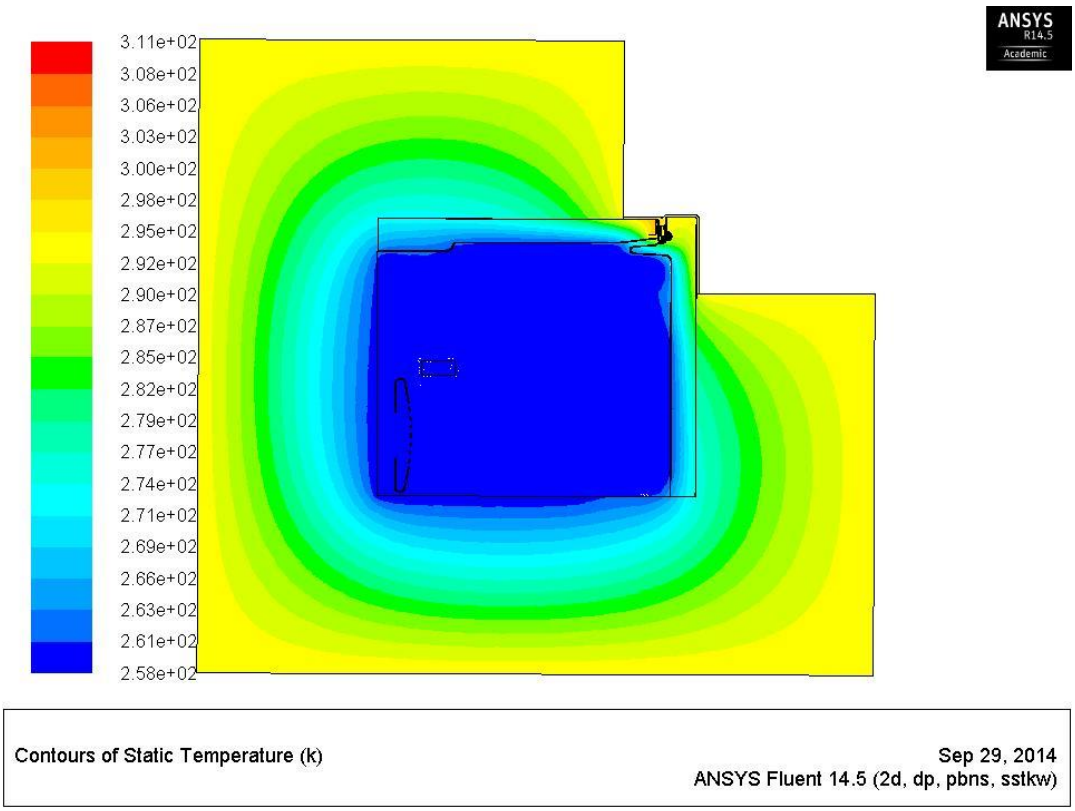


Figure 29: The temperature contour of the test cell with the hot pipe on.

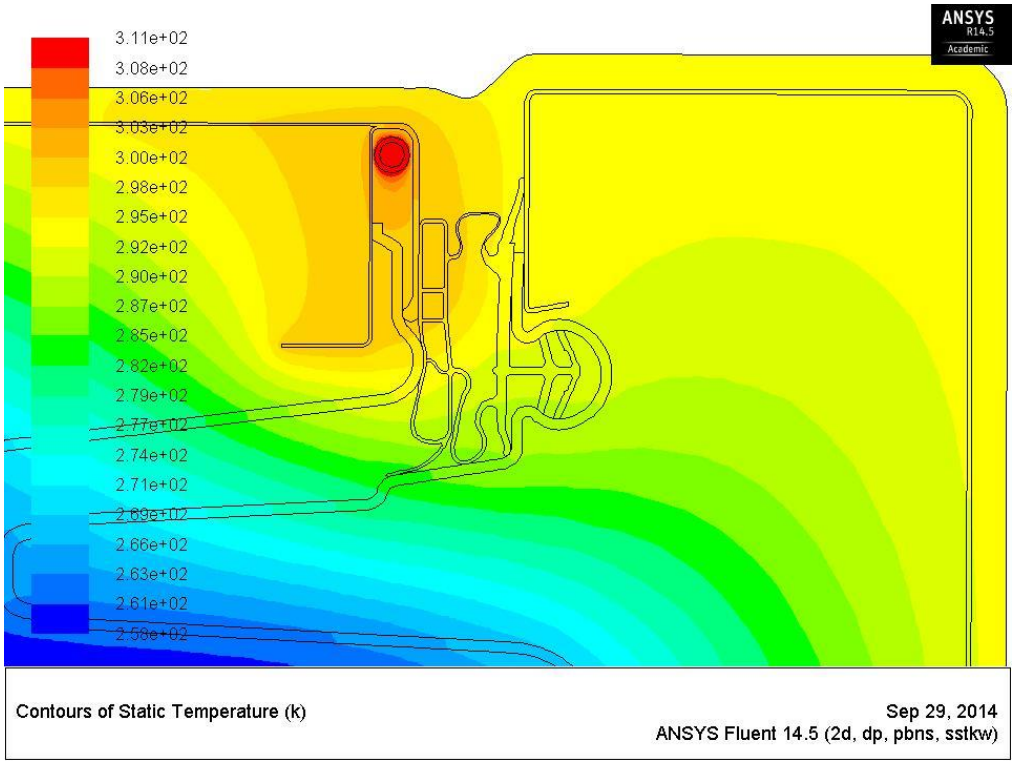


Figure 30: The zoomed in temperature contour at the gasket region with the hot pipe on.

## 7.6 The "Best Fit" Shape Profile Generated from the Simulations

In order to validate the simulation results presented above, corresponding experimentations are performed on the test cell, where six heat flux sensors are placed along the surface of the gasket region to measure the heat transfer rate [see Fig. 1 (a)]. The experimental data is gathered by Mr. Shervin Shoai Naini. In the present study, the CFD is used to "fill in" the heat flux profile between the six experimentally measured heat fluxes along the gasket region. The CFD is 2D and is therefore not expected to quantitatively predict the measurements. However, it is assumed that the CFD profile will have the qualitatively correct shape such that it can be scaled to best fit the experimental

measurements as discussed below. Before presenting the comparison between the results obtained from experiments and simulations, the coordinate used along the gasket region is presented in Fig. 31.

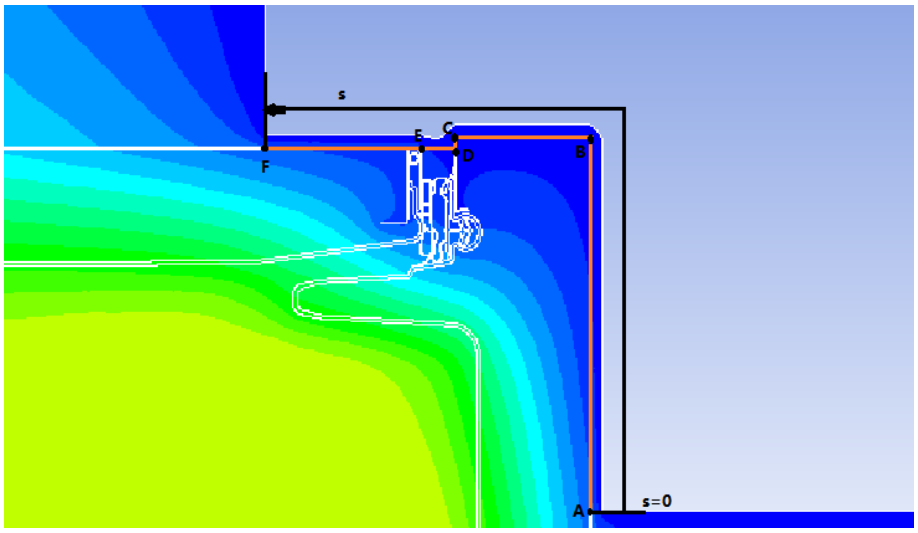


Figure 31: The coordinate used along the gasket region. The solid orange line represents the outer surface of the gasket region, whose origin is fixed at point A. The coordinate along the surface of the gasket region is "s". The location of the six heat flux sensors are placed along the s coordinate at locations 0.03 m, 0.09 m, 0.192 m, 0.258 m and 0.303 m.

A "best fit" profile is proposed and developed by using Least Square Error (LMSE) method. The "best fit" profile aims to fill the vacancy of missing experimental measurement points and provide a continuous heat flux curve that are convenient for any user to integrate to obtain the total heat loss by their own definition of the gasket region length.

The "best fit" profile is obtained by the LMSE method in the following procedure:

First, an initial heat flux profile along the gasket region is selected (e.g. the original gasket with 9.2 W heat load under the condition of natural convection). Secondly, the numerical points (e.g. $CFD_i$) obtained from the selected heat flux profile at corresponding six experimental measurement points (e.g. $Exp_i$) are extracted. A dimensionless scaling factor α is determined by minimizing the MSE in the following equation:

$$MSE = \sum(Exp_i - \alpha CFD_i)^2 \qquad (6.1)$$

The detailed process of obtaining the "best fit" profile is coded in FORTRAN and the codes are attached as an Appendix at the end of this thesis. The final "best fit" non-dimensional profiles are shown in Figs. 32 and 33 in dimensional and non-dimensional forms, respectively.

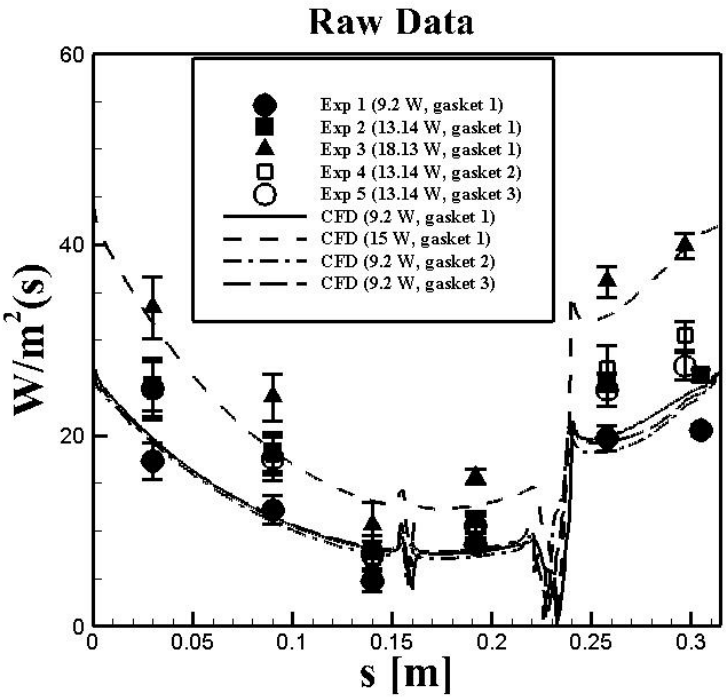


Figure 32: The plot of the continuous heat flux profile obtained from numerical simulations

and experimental data measured by six heat flux sensors along the gasket region surface. (The experimental data is the courtesy from Mr. Shervin Shoai Naini.)

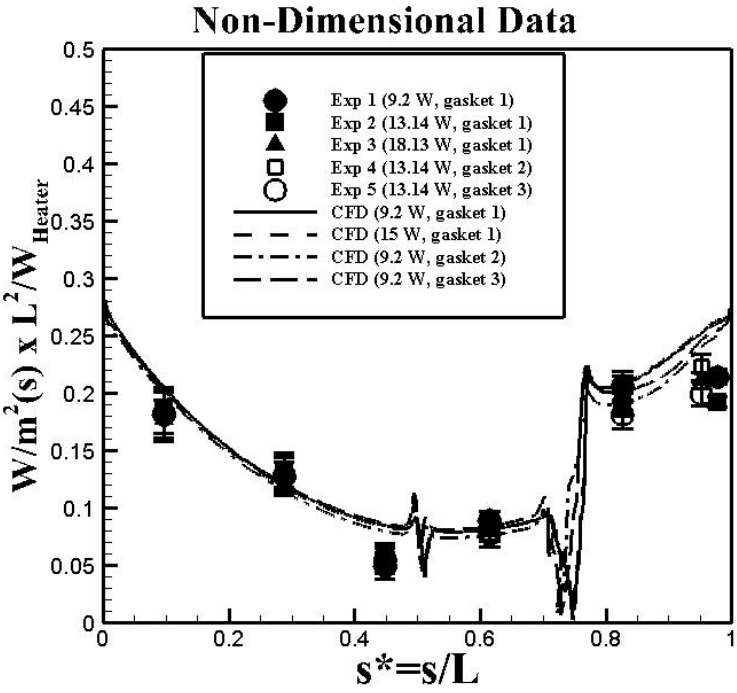


Figure 33: The "best fit" profile obtained by LMSE method. s* is obtained by dividing the position of the continuous points (s) by the length of the gasket region (l).

# CHAPTER 8: CONCLUSIONS

In the present study, numerical simulations (CFD) are carried out to systematically investigate the heat loss at the gasket region of the refrigerator. The simulations are conducted in support of an experimental test cell built to isolate the gasket region of refrigerators. The test cell allows for measurements of the heat leakages through the gasket region and measurements were made with heat flux sensors for three different gaskets. The primary objectives are to obtain the effective heat leakage in energy leakage per unit time, per unit length along the gasket, and per degree of temperature difference across the gasket (eg.W/m·K) and to be able to distinguish differences in heat leakages between different gaskets. Since only six heat flux measurement locations were possible, CFD is performed to provide "shape profiles" that can be best fit to the experimental data to provide a continuous heat flux distribution across the entire gasket region.

The CFD is also used to predict the relative changes to the heat leakages that occur due to other effects that either could not be incorporated into the test cell or could not be isolated. These include the effects of the hot loop found along the perimeter of a refrigerator's freezer section, the relative effect of radiation heat transfer, and the effect of forced convection from an evaporator fan. In summary, the heat leakage at the gasket increases 22 % when the electric fan is in operation. When radiation heat transfer is taken into consideration the numerical results increase by 11 %. The presence of the hot loop is found to increase the heat leakage by 18 %.

## APPENDIX

FORTRAN Code for Least Mean Square Error Analysis

```
PROGRAM FIT

PARAMETER(N=6,M=100,NMAX=1000)

real*8 X(N),Y(N),lms(NMAX)

real*8 dlta,maxa,mina,error,minerror

integer minnumber

mina=0.2d+00

maxa=2.d+00

dlta=(maxa-mina)/dble(float(NMAX-1))

C Input the six experimental heat flux measurements

X(1)=17.35

X(2)=12.22

X(3)=4.76

X(4)=8.57

X(5)=19.70

X(6)=20.54

C Input the CFD curve values at the same locations

Y(1)=19.66

Y(2)=11.44
```

```
Y(3)=8.15

Y(4)=7.82

Y(5)=19.93

Y(6)=25.06

do j=1,NMAX

a=mina+dlta*dble(float(j-1))

lms(j)=0.d+00

error=0.d+00

do i=2,N

error=(X(i)-a*Y(i))*(X(i)-a*Y(i))

lms(j)=lms(j)+error

enddo

enddo

do j=2,N

lms(j)=lms(j)/float(N)

end do

minerror=999.d+00

do j=1,NMAX

if(minerror.gt.lms(j))then
```

```
minerror=lms(j)

minnumber=j

endif

enddo

print*,minerror,minnumber,mina+dlta*dble(float(minnumber-1))

pause

end
```

## BIBLIOGRAPHY


1. Gupta, J.K., M. Ram Gopal, and S. Chakraborty, Modeling of a domestic frost-free refrigerator. International Journal of Refrigeration, 2007. **30**(2): p. 311-322.

2. Brent T. Griffith, D.A., Daniel Turler, Energy efficiency improvments for refrigerator/freezers using prototype doors containing gas-filled insulating systems. Proceedings of the 46 th International Appliance Technical Conference, USA, 15-17 May, 1995, 1995.

3. Xie, G. and P.K. Bansal, Analysis of defrosted water evaporation from three water trays in refrigerators. Applied Thermal Engineering, 2000. **20**(7): p. 651-669.

4. Majid Ghassemi, H.S., Review of energy efficiency of refrigerator/freezer gaskets. Environmental Protection Agency, EPA/600/S2-91/060, 1991.

5. Boughton, B.E., A.M. Clausing, and T.A. Newell, Investigation of household refrigerator cabinet thermal loads. HVAC and R Research, 1996. **2**(2): p. 135-148.

6. Shirley Flynn, K.R., Finite element analysis of heat transfer through the gasket region of refrigerator/freezer. Environmental Protection Agency, EPA/430/R-92/009, 1992.

7. Hasanuzzaman, M., R. Saidur, and H.H. Masjuki, Effects of operating variables on heat transfer and energy consumption of a household refrigerator-freezer during closed door operation. Energy, 2009. **34**(2): p. 196-198.

8. Hessami, M.-A. and A. Hilligweg. Energy Efficient Refrigerators: The Effect of Door Gasket and Wall Insulation on Heat Transfer. 2003. ASME.

9. Tao, W.-H. and J.-Y. Sun, Simulation and experimental study on the air flow and heat loads of different refrigerator cabinet designs. Chemical Engineering Communications, 2001. **186**(1): p. 171-182.

10. Bansal, P., E. Vineyard, and O. Abdelaziz, Advances in household appliances - a review. Applied Thermal Engineering, 2011. **31**(17-18): p. 3748-60.

11. Kim, H.S., J.S. Sim, and J.S. Ha, A study on the heat transfer characteristics near the magnetic door gasket of a refrigerator. International Communications in Heat and Mass Transfer, 2011. **38**(9): p. 1226-1231.

12. Huelsz, G., et al., Evaluation of refrigerator/freezer gaskets thermal loads. HVAC&R Research, 2011. **17**(2): p. 133-143.

13. Viet, T.P. and R. Furberg, heat transfer through gasket. Application for Technology Carrier, Electrolux, 2011.

14. Foster, A., et al., Measurement and prediction of air movement through doorways in refrigerated rooms. International journal of refrigeration, 2002. **25**(8): p. 1102-1109.

15. Tian, Y. and T. Karayiannis, Low turbulence natural convection in an air filled square cavity: part I: the thermal and fluid flow fields. International Journal of Heat and Mass Transfer, 2000. **43**(6): p. 849-866.

16. Laguerre, O. and D. Flick, Heat transfer by natural convection in domestic refrigerators. Journal of food engineering, 2004. **62**(1): p. 79-88.

17. Durmus, A. and A. Daloglu, Numerical and experimental study of air flow by natural convection in a rectangular open cavity: application in a top refrigerator. Experimental Heat Transfer, 2008. **21**(4): p. 281-95.

18. Bayer, O., et al., CFD simulations and reduced order modeling of a refrigerator compartment including radiation effects. Energy Conversion and Management, 2013. **69**: p. 68-76.

19. Laguerre, O., et al., Numerical simulation of air flow and heat transfer in domestic refrigerators. Journal of food engineering, 2007. **81**(1): p. 144-156.

20. Colomer, G., et al., Three-dimensional numerical simulation of convection and radiation in a differentially heated cavity using the discrete ordinates method. International Journal of Heat and Mass Transfer, 2004. **47**(2): p. 257-269.

21. Conceição António, C. and C. Afonso, Air temperature fields inside refrigeration cabins: A comparison of results from CFD and ANN modelling. Applied Thermal Engineering, 2011. **31**(6): p. 1244-1251.

22. Fukuyo, K., T. Tanaami, and H. Ashida, Thermal uniformity and rapid cooling inside refrigerators. International journal of refrigeration, 2003. **26**(2): p. 249-255.

23. Ding, G.-L., H.-T. Qiao, and Z.-L. Lu, Ways to improve thermal uniformity inside a refrigerator. Applied thermal engineering, 2004. **24**(13): p. 1827-1840.

24. Yang, K.-S., et al., An investigation of a top-mounted domestic refrigerator. Energy Conversion and Management, 2010. **51**(7): p. 1422-1427.

25. Smale, N., J. Moureh, and G. Cortella, A review of numerical models of airflow in refrigerated food applications. International Journal of Refrigeration, 2006. **29**(6): p. 911-930.

26. Jae Seong, S. and H. Ji Soo, Experimental study of heat transfer characteristics for a refrigerator by using reverse heat loss method. International Communications in Heat and Mass Transfer, 2011. **38**(5): p. 572-6.

27. Ansys Fluent theory manual 14.0 ed. Ansys Inc.

28. Patrick Oosthuizen, David Naylor. Introduction to Convective Heat Transfer Analysis. WCB/McGraw-Hill, 1999: p. 343-348.

29. B. E. Launder and D. B. Spalding. Mathematical Models of Turbulence, Academic Press, 1972.

30. David C. Wilcox. Turbulence Modeling for CFD . D C W Industries; 3rd edition, 2006.

31. Erhan Pulat, Mustafa Kemal Isman , Akin Burak Etemoglu, and Muhiddin, Effect of Turbulence Models and Near-Wall Modeling Approaches on Numerical Results in Impingement Heat Transfer, Numerical Heat Transfer, Part B: Fundamentals: An International Journal of Computation and Methodology, 2001. **60**(2), p. 486-519.

32. Joel H. Ferziger and Milovan Peric. Computational Methods for Fluid Dynamics. Springer-Verlag, third edition, 2001.

33. Pieter Verboven, Nico Scheerlinck, and Josse De Baerdemaeker, Computational fluid dynamics modeling and validation of the isothermal airflow in a forced convection oven. Journal of Food Engineering ,2000. **43**(1): p. 41-53.

34. Menter, F. R., "Two-Equation Eddy-Viscosity Turbulence Models for Engineering Applications," AIAA Journal, 1994. **32**(8): p. 1598-1605.

35. N. EL Gharbi, R. Absi, A. Benzaoui, and E.H. Amara. Effect of near-wall treatment on air flow simulations proceedings of 2009 International Conference on Computational Methods for Energy Engineering and Environment: ICCM3E. Sousse, Tunisia, 20-22, November 2009, p.185-189.

36. Salim. M. Salim, S.C. Cheah. Wall y plus strategy for dealing with wall-bounded turbulent flows. Proceedings of the International MultiConference of Engineers and Computer Scientists 2009. IMECS 2009, March 18 - 20, 2009, Hong Kong.

37. M.M.Noor, Andrew P. Wandel, Talal Yusaf. Detail guide for CFD on the simulation of biogas combustion in bluff-body mild burner. ICMER2013, Kuantan, Malaysia 1-3 July.